frontiers | Frontiers in Environmental Science

TYPE Original Research
PUBLISHED 02 February 2026
DOI 10.3389/fenvs.2025.1735866

OPEN ACCESS

EDITED BY
Alessandro Michele Hering,
Federal Office of Meteorology and Climatology, Switzerland

REVIEWED BY
Jingyu Wang,
Nanyang Technological University, Singapore
Tomeu Rigo,
Servei Meteorologic de Catalunya, Spain

*CORRESPONDENCE
Agostino Manzato,
agostino.manzato@arpa.fvg.it

RECEIVED 30 October 2025
REVISED 19 December 2025
ACCEPTED 22 December 2025
PUBLISHED 02 February 2026

CITATION
Manzato A, Knight C, Kumjian MR, Stenni B, Dreossi G, Masiol M, Zhang Q, Lin X and Heymsfield A (2026) A comprehensive description of the 1 August 2021 Azzano Decimo hailstorm in northeastern Italy. *Front. Environ. Sci.* 13:1735866. doi: 10.3389/fenvs.2025.1735866

A comprehensive description of the 1 August 2021 Azzano Decimo hailstorm in northeastern Italy

Agostino Manzato[1,2]*, Charles Knight[3], Matthew R. Kumjian[4], Barbara Stenni[5], Giuliano Dreossi[5], Mauro Masiol[5], Qinghong Zhang[6], Xiangyu Lin[6] and Andrew Heymsfield[3]

[1]OSMER, ARPA Friuli Venezia Giulia, Palmanova, Italy, [2]ISAC, Consiglio Nazionale delle Ricerche, Bologna, Italy, [3]Mesoscale and Microscale Meteorology Laboratory, National Center for Atmospheric Research, Boulder, CO, United States, [4]Department of Meteorology & Atmospheric Science, The Pennsylvania State University, University Park, University Park, PA, United States, [5]Department of Environmental Sciences, Informatics and Statistics, Ca' Foscari University of Venice, Venice, Italy, [6]Department of Atmospheric and Oceanic Sciences, Peking University, Beijing, China

On 1 August 2021, a vigorous hailstorm hit Azzano Decimo, in northeastern Italy. The supercell storm produced hailstones up to 10 cm in maximum dimension, which is quite unusual in this area. The storm's environment registered one of the largest potential instabilities (>3400 J kg^{-1}) ever observed by the local operational Udine radiosonde site. In this paper, we analyze the mesoscale environment supporting the hailstorm. Observations from the nearby operational Fossalon di Grado dual-polarization radar showed the presence of a pronounced Bounded Weak Echo Region and differential reflectivity column, both proxies for intense updrafts; however, Doppler velocities revealed only weaker winds, with the mesocyclone mostly confined to midlevels. Two independent observers in Azzano Decimo collected nine hailstones, including one with a maximum dimension of 9 cm. The physical structure of these hailstones was analyzed in the National Center for Atmospheric Research cold room, including normal and cross-polarized light photographs of thin sections to identify the different growth layers inside each hailstone. Additionally, ice samples were taken from 1 cm × 1 cm × 1 mm pieces from these thin slices. The stable isotopic ratio analyses were performed on these specimens using a Picarro cavity ring-down spectrometer. Isotopic content of the hailstone layers revealed significant variability, including some internal layers that showed signs of kinetic fractionation owing to evaporating liquid being incorporated into the growth layer, likely from evaporation of surface liquid during wet growth or collection of recirculated raindrops that experienced evaporation prior to participating in hail growth. Despite such large isotope variability, the Jouzel model analysis suggested that the major growth happened at high altitudes (between 8 and 10 km), which is also in agreement with a reversible-adiabatic parcel model and radar observations from the event.

KEYWORDS

hailstone analysis, hailstorm structure, stable water isotopes, ICM isotopic cloud model, radar

1 Introduction

In general, hail is particularly frequent in the Po Valley (Morgan, 1973). In fact, satellite analyses have confirmed that northern Italy is a European hot spot for hailstorms (Punge et al., 2017). Moreover, northern Italy also features a relative maximum in climatologies of lightning flashes (Taszarek et al., 2020), particularly in the northeastern part or Friuli Venezia Giulia (hereafter FVG; Manzato et al., 2022b). In this region (see Figure 1) the low bathymetry Adriatic Sea and lagoons come very close to the Alpine chain, with peaks reaching 2,800 m AMSL, favoring the orographic lifting of moisture. A hailpad network has been operating in FVG since 1988 (see analyses of these data by Giaiotti et al., 2001; Manzato, 2012; Manzato et al., 2022a). In an analysis of thousands of hailpad observations and nearly 7.5×10^5 hailstone dents it was found that FVG hailpads very rarely observe hailstones with equivalent spherical diameters >4 cm (Manzato et al., 2022a). However, by accounting for the undersampling bias from small-area hailpads following the methods of Smith and Waldvogel (1989) or Grieser and Hill (2019), the maximum dimensions of hail "in the vicinity" are estimated to be in the 6–9 cm range. That study also showed an increasing trend for hail size and a seasonal peak for hail size and kinetic energy flux in the first part of August. Thus, although known as a hot spot for hail, observations of extremely large hailstones are relatively sparse.

At about 5 UTC on 1 August 2021, the village of Azzano Decimo (FVG, NE Italy, see Figure 1) was hit by a severe hailstorm that produced hail up to giant size (Blair et al., 2011, i.e., 10 cm in maximum dimension). Although the case analyzed in this study is from the 1 August 2021 event, very recently (24 July 2023), the village of Azzano Decimo once again raised the attention of the international hail community. A storm there produced the new European hail size record: pictures of a hailstone with an estimated ~19 cm maximum diameter[1], reaching "gargantuan" status (Kumjian and Co-authors, 2020), the first of its kind documented in Italy and the new European hail size record. Thus, although hail >9 cm is considered exceptional in this region (Manzato et al., 2022a), these storms lend credence to the recent additive logistical modeling study by Battaglioli et al. (2023), which suggests northeastern Italy is experiencing the greatest increases in large hail occurrence in the last decade, with an overall tripling of significantly severe (>5 cm) hail frequency since 1950. Those authors found that the increasing hail occurrence is driven primarily by increases in low-level moisture and instability. Moreover, Battaglioli et al. (2023) was based on ERA5 reanalysis data (Hersbach et al., 2020), whereas Manzato et al. (2025) showed that the increasing trends of instability and moisture derived from high-resolution soundings in northeastern Italy are even larger than those derived from the ERA5 reanalysis.

This case affords a unique opportunity to take a closer look at storms producing giant hail in this region, perhaps exemplifying the recent trends inferred from modeling studies and environmental analyses. This involves a detailed mesoanalyses of the environment leading up to and supporting the storm, as well as radar analysis of the storm's structure. Fortunately, several hailstones observed on 1 August 2021 in Azzano Decimo were preserved, and are the largest and most well-documented specimens ever collected in the FVG region. A unique international/multi-continental collaboration allowed for detailed analysis of hailstone specimens collected from this event. In particular, nine of these hailstones were collected by two observers living in Azzano Decimo and sent to the U.S. National Center for Atmospheric Research (NCAR) for a evaluation of their internal physical structure (e.g., Knight and Knight, 1968; Knight and Knight, 1970b). Moreover, many specimens were taken from the different growth layers to analyze their isotopic composition. These analyses provide at least qualitative insights into the structure of the hailstones and their growth history. The novelty of this study is in the diversity of datasets synthesized for better understanding a giant hail event–one of the first studies to put together the disparate pieces of the puzzle for a comprehensive analysis.

In the following Section, the hailstone data and analysis methods are described. Section 3 describes the meteorological conditions leading to the supercell storm that produced these hailstones. In particular, data from surface stations, radar, soundings, and satellite are used to describe the environment associated with these large hailstones. Radar and sounding results are briefly compared with those of the record-breaking 24 July 2023 case. Section 4 describes the results of the hailstone analysis, including both a physical and chemical analysis. Lastly the Conclusions summarizes the main results found.

2 Data and methods

2.1 Hailstone collection

After the hailstorm, two citizens of Azzano Decimo (Michele Cristofoli and Sara Santarossa) collected some of the largest hailstones from their garden and put them into their freezers. Figure 2a shows a wide distribution of hail sizes at the observer's location. Of course, the observer collected only the largest stones (Figure 2b). Figure 2c was taken by the other observer two days later, when she decided to weigh the hailstones. ARPA FVG - OSMER (Osservatorio Meteorologico dell'Agenzia per l'Ambiente del Friuli Venezia Giulia) discovered the existence of these 9 hailstones thanks to social media and, a few months later, organized their shipping with 60 kg of dry ice (see the Supplementary Figure S1) to NCAR in Boulder, Colorado, United States, where a cold room laboratory is operated by one of the authors (Knight).

2.2 Hailstone analysis

2.2.1 Sectioning the Italian hailstones

Once received at NCAR, the two groups of hailstones (hereafter "C" for those from Cristofori and "S" for those from Santarossa) have their approximate maximum dimension, minimum dimension, and mass measured (Table 1). They are then sectioned according to the following procedure. First, using a band saw in the cold room, a cut through the stone was made.

1 https://www.essl.org/cms/hail-record-broken-again-19cm-hailstone-confirmed-in-italy/

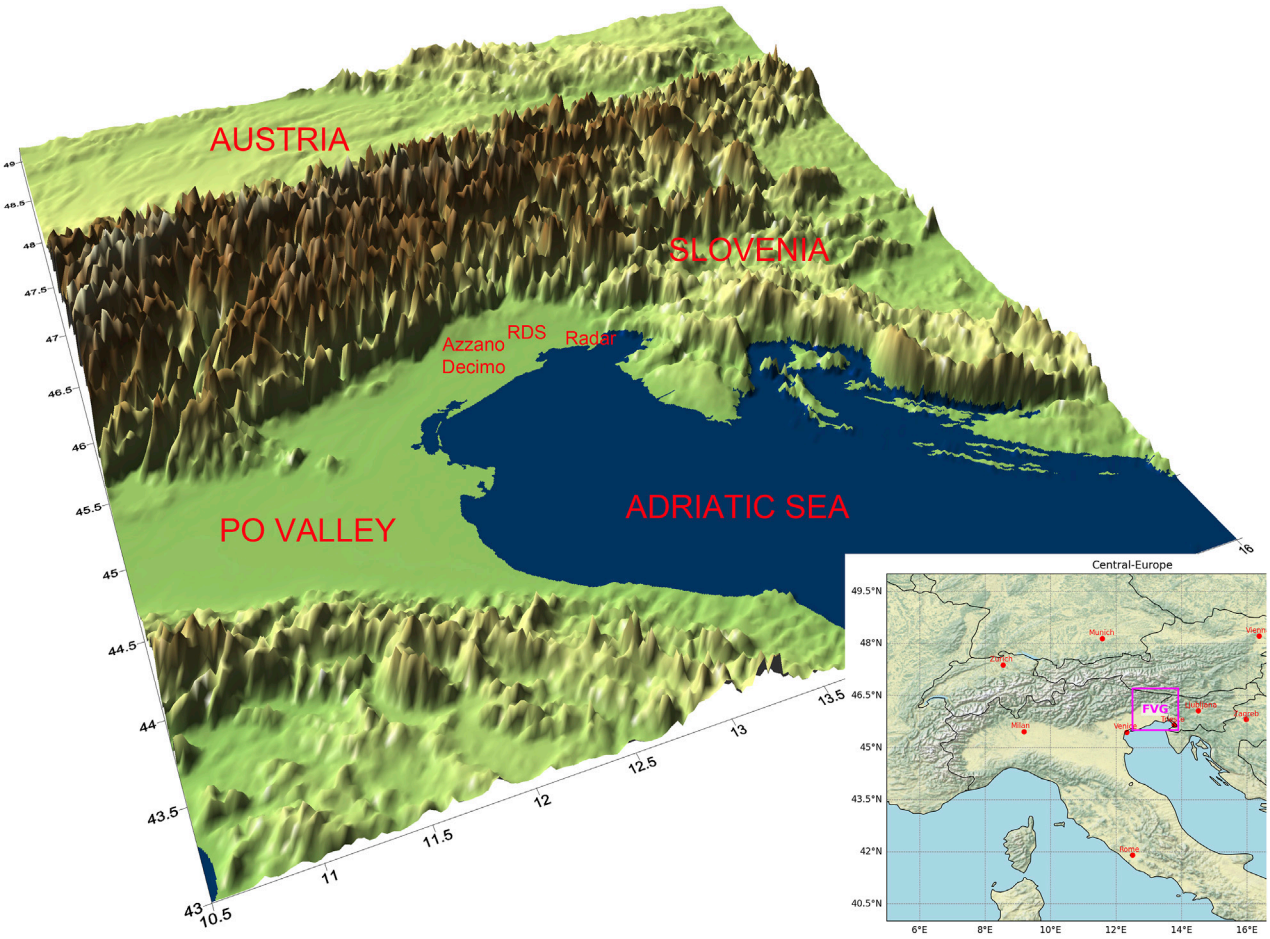

FIGURE 1
Northeastern Italy domain with stylized 3D orography and the location of Azzano Decimo, Udine radiosounding (RDS) and Fossalon di Grado radar ("Radar"). In the bottom-right corner the location of the FVG region with respect to Central Europe is highlighted.

An attempt was made to have the hailstone's maximum and minimum dimensions, as well as its growth center, in the plane of the cut, although this can be difficult in practice. After the initial cut, a parallel cut is made to produce a slice about 3–5 mm thick. These thick slices are used for photographing to analyze the growth layers. Another parallel cut from one of the remaining halves of the stone was made, this time ~200 – 300 μm thick. These "thin sections" are used to examine the internal crystalline structures via photography with crossed polarizing filters.

Hailstones S4 and S5 were solidly frozen together during shipping. Prior to analysis, they were broken apart and the section of ice that attached them trimmed. Unfortunately, the original thick section of S4 was dropped and broke apart upon impact with the cold room floor. A new S4 section was made from the remaining half that looked to include the closest of the two to the growth center.

2.2.2 Preparing samples for water isotope analysis

After photographing the thick and thin sections, samples were taken from the hailstone thick sections for isotopic analysis. The samples were taken from 2-cm-wide strips through the growth centers of the sections. Decisions about how to sample were made while inspecting the actual thick sections in the cold room, which can be rather different from inspecting the photographs of the thick sections. The samples were placed in vials and shipped back to Italy, where they were analyzed with a cavity ring-down spectrometer Picarro L2130-i set in liquid mode (Supplementary Figure S2). Details of the instrumental setup, analytical protocols and precision are reported in Supplementary Material S1.

We emphasize that any simple interpretation of the isotopic results is built on an assumption that the isotope fractions in the ice represent those that were present in the cloud water; in reality, this assumption can be dubious, particularly so in the clear ice layers from wet growth. During wet growth, liquid exists on the surface of the hailstone, which may promote isotope exchange with the environment and isotope fractionation during freezing that cause isotope ratios to differ from those in the cloud droplets. If raindrops participate in hailstone growth (as in, e.g., Kumjian and Lombardo, 2020), the assumption is even worse given that raindrop isotope content can be substantially different from that of nearby cloud droplets (e.g., Friedman et al., 1962; Macklin et al., 1970; Ehhalt and Östlund", 1970; Knight et al., 1975) Further, several additional assumptions are made, as outlined in (for example) Macklin et al. (1977):

FIGURE 2
Photographs from the two observers that collected the 9 studied hailstones. Photographs **(a)** and **(b)** are from Michele Cristofoli at 520 UTC on 1 August 2021, featuring freshly fallen hail; photograph **(c)** by Sara Santarossa at 1700 UTC on 3 August 2021, after the hailstone was preserved in a freezer for 2 days.

- There is no entrainment of free-tropospheric air into the updraft as the air in the updraft ascends. We know this is not true (e.g., Nowotarski et al., 2020; Lin and Kumjian, 2022), but its quantification is difficult. In principle, if the amount of entrainment can be determined, the model can be updated accordingly.
- The isotope content of air feeding the storm does not change throughout its lifetime—this is hard to know without isotope measurements of the water vapor in the air, which usually are not available.
- The water vapor mixing ratio of the air feeding the storm does not change throughout its lifetime—again, this is probably not true and often not well quantified.
- Cloud droplets are in isotopic equilibrium with the water vapor in the air as they ascend—some experimental evidence and theoretical considerations suggest this is probably true in most cases (e.g., Jouzel and Merlivat, 1984), except perhaps in the most extreme updrafts where large supersaturations are possible (e.g., Lebo et al., 2012).
- Air feeding the storm updraft originates from a well-mixed boundary layer in which the vapor content and isotopic content of vapor are uniform: in many cases this is mostly true, but not always. Further, air from above the boundary layer is often ingested into storms (see point 1).
- These hailstones were conserved by the two observers in their freezer without special precautions, thus there could have been some contamination or sublimation in that environment, though restricted to the outermost layers of the hailstones.

Despite these limitations, we can still gain at least some qualitative insights from the isotopic composition of the hailstones (e.g., Lin et al., 2025), and do so with the aforementioned caveats in mind.

2.3 Meteorological analysis

Multiple kinds of observations are used to analyze the meteorological conditions supporting the Azzano Decimo hailstorm, including data from surface meteorological stations, radiosondes, radars, satellite, and lightning sensors. The surface stations are managed by Civil Protection FVG, while the data quality control is made by ARPA FVG - OSMER. The highest-resolution sampling time is 1 min, but in this work only station measurements with 5-min resolution are used. The radiosounding data are managed by Aeronautica Militare. The Rivolto station (45.978° N, 13.058° E, 51 m AMSL; WMO ID 16045) usually performs only 00 and 12 UTC soundings, but, upon request of ARPA FVG - OSMER during alerts or severe weather outlook, they can also launch extra soundings at 06 and/or 18 UTC, as was done in the Azzano Decimo case. The sondes used are Vaisala RS41 and the full-vertical resolution data (1-Hz sampling) are analyzed. Two Doppler C-band radars cover the area of interest: the first is the Fossalon di Grado GPM-500C dual-polarization radar (45.73° N, 13.48° E, 0 m AMSL, see Bechini et al., 2002), which is managed by Civil Protection FVG and operates at 5.630 GHz (wavelenghth ~5.3 cm) with an unambiguous range of 125 km, and the Pasja Ravan single-polarization radar (46.10° N, 14.23° E, 1,019 m AMSL), managed by the Slovenian Environmental Agency (ARSO) and

TABLE 1 Size and mass of 9 hailstone samples collected during the 1 August 2021 event.

Hailstone ID	Maximum dimension (cm)	Minimum dimension (cm)	Mass (g)
S1	8	4	120
S2	6	5	80
S3	7	5	103
S4	7.5	4.5	110
S5	7.5	4.5	110
C1	5	3	40
C2	7	4	100
C3	8.5	3	80
C4	7.5	5	165

operating at 5.633 GHz with an unambiguous range of 150 km. While the Pasja Ravan radar is 120 km far from Azzano Decimo, the Fossalon di Grado is much closer and, when scanning the volumes every 5 min, was recently ranked as one of the best radars in Europe for mesocyclone detection (van 't Veen and Groenemeijer, 2025). Lightning data were purchased from the Meteorage company, which uses Vaisala LS7002 lightning detection sensors that are able to report both cloud-to-ground and cloud-to-cloud flashes with good accuracy (Erdmann et al., 2020). More technical details on lightning detection in this area can be found in Manzato et al. (2022b) and reference therein. Satellite data in different channels are from the EUMETSAT MSG dataset (see https://www.eumetsat.int/msg-services).

3 Results & discussion

3.1 Synoptic analysis

Prior to the event, the ECMWF IFS ERA5 reanalysis for 06 UTC 1 August 2021 showed a 500-hPa trough upstream, centered on France (Figure 3a). 500-hPa temperatures between −12 and −14 °C have overspread northeastern Italy. At 700 hPa, strong southwesterly flow associated with the trough helped transport moist Mediterranean air towards the Italian peninsula, resulting in large relative humidity near the Alps and Appenines mountains (Figure 3b). In northeastern Italy, winds showed consistent uplift associated with forcing for ascent from the approaching trough. The FVG region was within and on the cool side of a diffuse baroclinic zone associated with almost stationary cold front (not shown).

3.2 Thermodynamic and kinematic vertical profile analysis

Figures 4a–c show Thetaplot diagrams (Morgan, 1992) for three consecutive soundings taken on 1 August 2021 from Aeronautica Militare in Udine–Rivolto, located approximately 86 km to the northeast of Azzano Decimo. Throughout the entire 18 – h period shown, the atmosphere over northeastern Italy was potentially unstable. CAPE increased from 821 J kg^{-1} at 00 UTC to 3444 J kg^{-1} by 06 UTC. This latter measurement ranks among the top 10 highest values ever observed at Udine (with a record dating back to 1992). The extremely large potential instability is supported by a low-level (0–2-km AGL) moist layer featuring Θ_e up to 352 K, overlaid with low Θ_{es} in the mid levels. Indeed, the high Θ_e values at low levels are also confirmed by surface observations at this time, which show significant advection of high-Θ_e air from the Adriatic Sea (Supplementary Figure S3). Note that the exact Θ_e values and computed CAPE must be considered with care, because part of the 06 UTC sounding was already contaminated by clouds; the profile is almost saturated with respect to liquid water above 750 hPa, meaning that convection in the vicinity was already ongoing at the time of sounding launch, at ~05 UTC. The very low values of Θ_{es} in the saturated part of the sounding would increase the CAPE computed relative to a sounding not in cloud. For example, compare the large part of the Θ_{es} profile below 330 K at 06 UTC with the much smaller part having Θ_{es} < 330 K in the 00 UTC sounding. The decrease in 500 hPa temperature from −11.6 °C to −14.1 °C from 00 UTC to 06 UTC and consequent increase of instability can be partly due to this contamination effect, but there was also cold-air advection (from the south-southwest) in the mid troposphere (cf. Figure 3b).

Focusing on the wind profiles in Figure 4, we see that the 700-500-hPa layer has a mean wind of 21 m s^{-1} from about 210° (SSW) at both 00 and 06 UTC. On the other hand, the lowest 500 m AGL reveals a wind shift from 67° to 190° from 00 to 06 UTC. The significant veering of the low-level winds from east-northeasterly to south-southwesterly during this period marks the retreat of the surface frontal boundary and helps advect moist maritime air from the Adriatic sea inland, contributing to the increase in instability over this period. More generally, the lowest winds shown in Figure 4b suggest that the storm inflow was fed by maritime air. Additionally, by 06 UTC there is weaker shear, both in low levels (e.g., sfc–3-km bulk shear decreases from 14.7 to only 6.0 m s^{-1}) and in the 1 – 6-km layer (bulk shear decreasing from 27 m s^{-1} to 21 m s^{-1}), while the hodograph featured less turning at low levels. Both weaker low-level shear and "straighter" hodographs are thought to be favorable environmental conditions for hail production (e.g., Kumjian and Lombardo, 2020; Kumjian et al., 2021; Nixon et al., 2023; Lin and Kumjian, 2026).

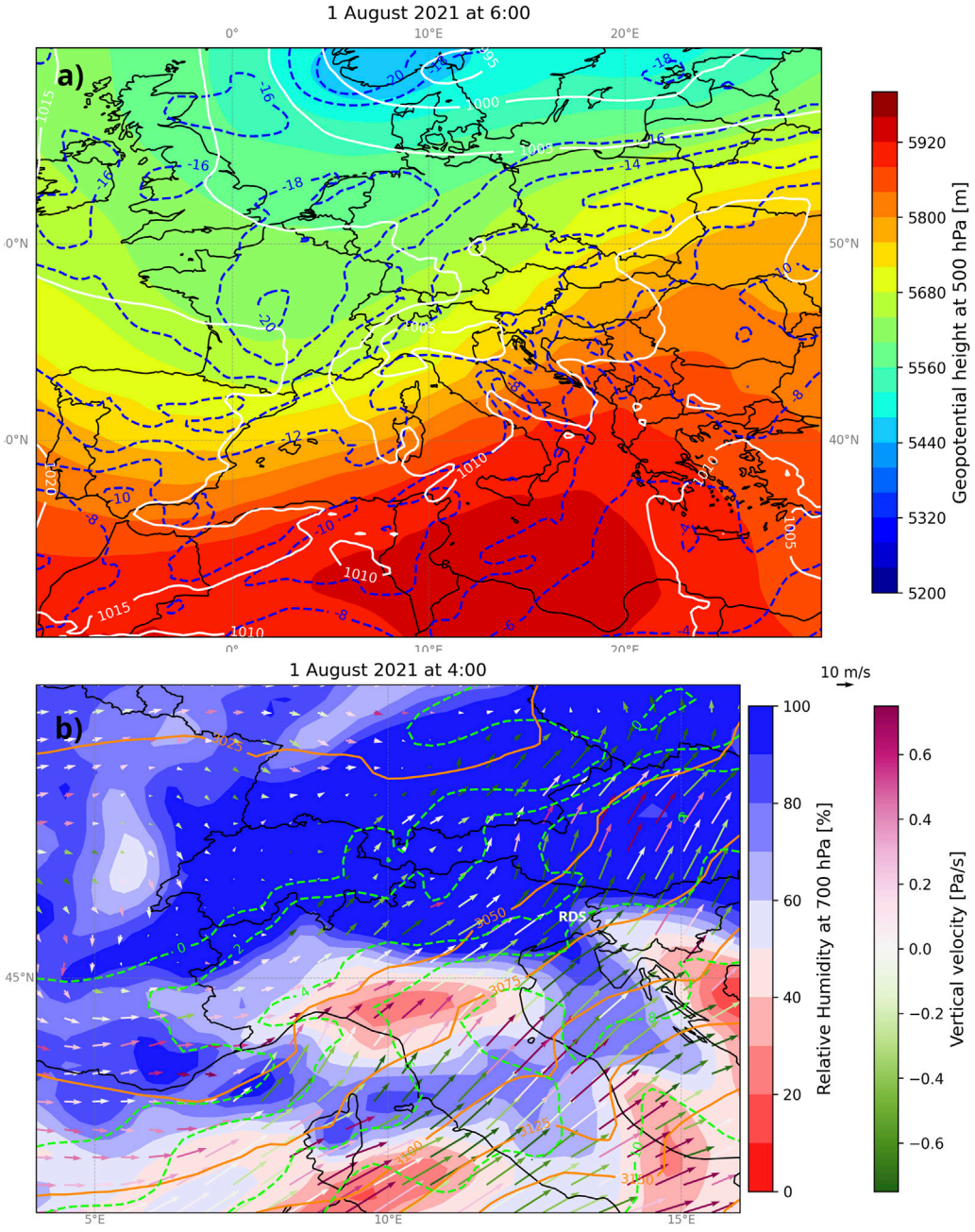

FIGURE 3
Synoptic situation as described by ECMWF ERA5 reanalysis valid 06 UTC on 1 August 2021. **(a)** 500-hPa geopotential height (shaded, in m), 500-hPa tempeature (blue dashed contours in 2- ˚C increments), and surface pressure (white contours in 5-hPa increments). **(b)** Note zoomed-in view centered on northern Italy. Fields shown are 700-hPa relative humidity (%, shaded in red/blue according to left outset scale), 700-hPa geopotential height (orange solid contours in m, in 25-m increments), and temperature (dashed green contours in 2- ˚C increments. 700-hPa horizontal wind vectors are also overlaid, colored by pressure vertical velocity (Pa s^{-1}, shaded in purple/green according to right outset scale). Purple vectors indicate descent and green vectors indicate ascent. Courtesy of Francesco Sioni, OSMER - ARPA FVG.

Because of the partial convective contamination of the 06 UTC Udine sounding, we extracted an uncontaminated profile from the ERA5 reanalysis at 04 UTC, at the grid point closest to Azzano Decimo. (Surrounding gridpoints were also examined, and the profiles do not change considerably.) Using the radar-estimated storm motion (7.8 m s^{-1} from 260˚), we constructed a storm-relative hodograph (Figure 4d). The storm-relative hodograph exhibits numerous features thought to be conducive to hail production in supercell storms (e.g., Kumjian and Lombardo, 2020; Nixon et al., 2023; Lin and Kumjian, 2026), including being mostly straight, having weak sfc–1-km shear (4.3 m s^{-1}) paired with strong 1 – 6-km shear (25.9 m s^{-1}). Further, additional shear in the 6–9 km layer could contribute to increasing updraft area (Warren et al., 2017), analogous to the increase in updraft area with increasing sfc-6-km shear (e.g., Dennis and Kumjian, 2017). Increased updraft area is known to be conducive to hail

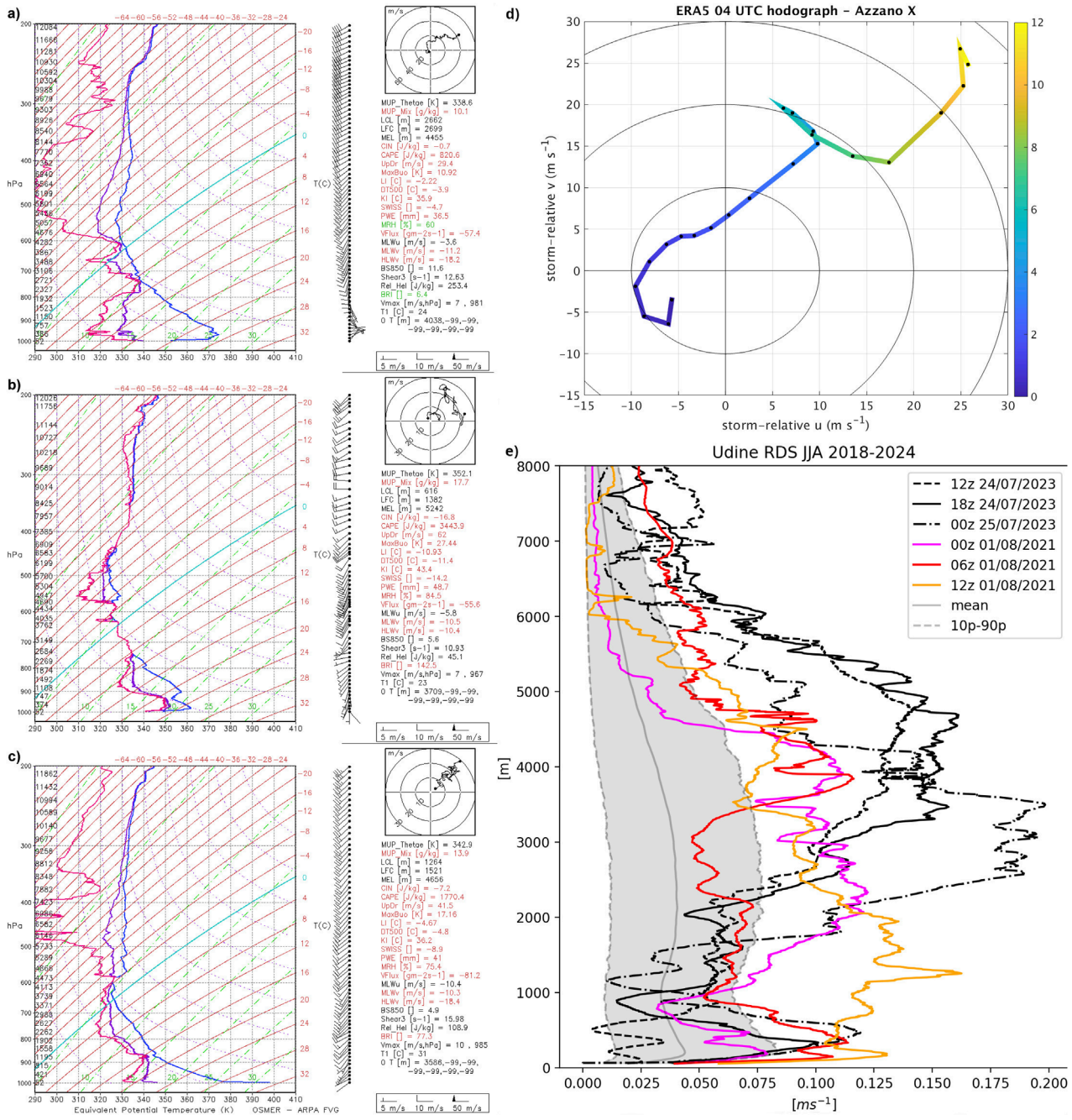

FIGURE 4
Thetaplot of Udine–Rivolto soundings at **(a)** 00, **(b)** 06, and **(c)** 12 UTC. The blue lines are the saturated equivalent potential temperature (Θ_{es}) profiles, red lines are the equivalent potential temperature (Θ_e) profiles, and the purple lines are the dewpoint equivalent potential temperature (Θ_{ed}). Wind barbs are shown to the right. Outset hodographs and lists of derived parameters are provided next to each panel. **(d)** Storm-relative hodograph constructed using data from the 04 UTC ERA5 reanalysis. Color indicates altitude AGL. **(e)** *VT* profile of Udine–Rivolto soundings on 1 August 2021 and on 24 July 2024 compared to 10th-90th percentiles of the JJA 2018–2024 distribution. Panel **(e)** courtesy of Francesco De Martin, Bologna Univ., adapting Figure 7 of De Martin et al. (2025).

production by providing longer possible residence times for growing hailstones (e.g., Nelson, 1983; Kumjian and Lombardo, 2020; Kumjian et al., 2021; Lin and Kumjian, 2022; 2026). The subtle weakening of the midlevel storm-relative flow component perpendicular to the ~2 – 6-km shear vector has been recently shown to favor hail production by promoting weaker horizontal winds along a favorable hail trajectory within the updraft (Lombardo and Kumjian, 2025).

De Martin et al. (2025) recently found that the Udine soundings associated with the record-breaking hailstone on 24 July 2023 had exceptional profiles of water-Vapor Transport ($VT = V \times q_v$, where V is horizontal wind speed and q_v is vapor mixing ratio), well

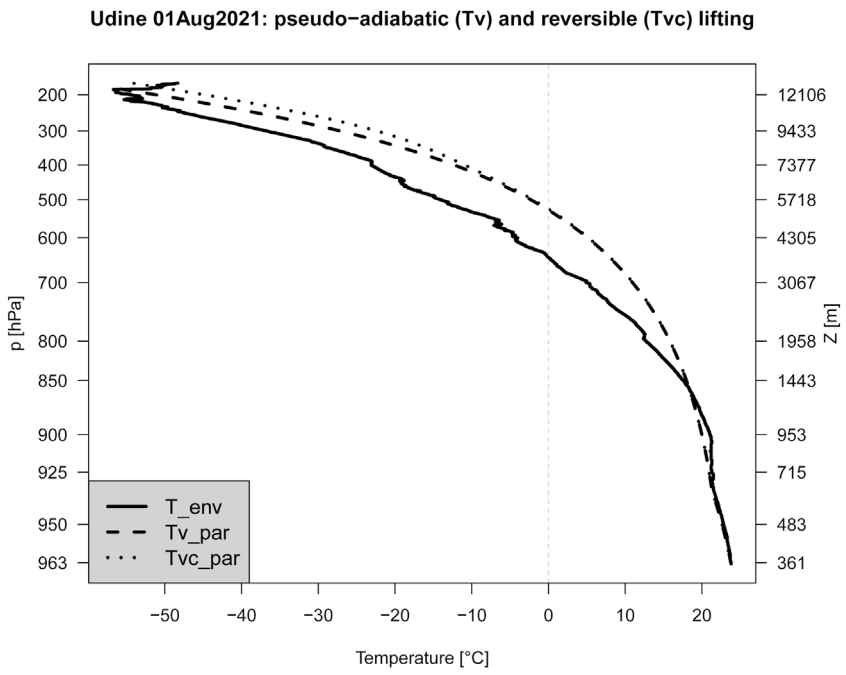

FIGURE 5
The 06 UTC sounding temperature (T_{env}, solid line) and the lifted parcel temperature using pseudoadiabatic lifting ("Tv_{par}", black dashed line) or reversible adiabatic lifting ("Tvc_{par}", black dotted line), from the initial height of the most-unstable parcel (which originates at ~360 m MSL) to the equilibrium level. The LCL is located at 614 m MSL, whereas the LFC is at about 1,100 m MSL.

exceeding the summertime (June, July, August) climatological values from 2018-2023. Their statistical study showed that *VT* is particularly skilled in discriminating large hail. Hence, we investigate if the first August 2021 *VT* values were also particularly high. Figure 4e shows that the 00 and 12 UTC soundings had particularly high *VT* values between 0.1 and 4.5 km AGL, including >0.1 m s^{-1} between 2 and 4.5 km at 00 UTC and between 0.1 and 2.5 km at 12 UTC. Even the partially contaminated sounding of 06 UTC has *VT* values above the 90-percentile (~0.08 m s^{-1}) of the updated JJA 2018–2024 distribution between 0.1 and 0.6 km (S-SW low-level jet feeding the storm inflow) and between 3.5 and 5 km AGL. However, the exceptional *VT* values in the mid-troposphere reached during 24 July 2023 were not equaled on 1 August 2021.

Of importance for hailstone growth is an understanding of the mixed-phase region within the cloud, which can differ substantially from the ambient environmental air in cases with extremely large instability such as this one. We can apply parcel theory to the 06 UTC sounding and obtain a rough estimate of the temperature profile experienced by the 30 hPa-high most unstable parcel, which is centered at 964 hPa (~360 m AGL). Figure 5 shows the environmental profile (continuous line) and the lifted parcel profiles computed assuming 1) pseudoadiabatic ascent using the "Tv" method described in Manzato and Morgan (2003) (dashed), and 2) reversible adiabatic ascent (i.e., rising parcel retains all condensed water), using the "Tvc" method described in the same work (dotted). In both cases, the lifted parcel experiences temperatures <0 °C above 5.2 km, whereas the homogeneous freezing point (~−38 °C) is reached at 10.7 km and 11.4 km, respectively, for the "Tv" and "Tvc" methods. These altitudes are approximately 1-2 standard deviations above the mean most-unstable parcel glaciation level heights reported in Spychalla and Kumjian. (2025b) for a large dataset of significantly severe supercell storms in the U.S (Warren et al., 2021). Given that severe storm environments in Europe tend to be less extreme than those in the U.S. (e.g., Taszarek et al., 2020), these results suggest the potential for a particularly intense and deep storm with an in-cloud mixed-phase region likely is between about 5 and 11 km.

3.3 Mesoscale analysis

3.3.1 Satellite and station analysis

In this Section we will use satellite and station data to describe the hailstorm path and the exact timing of the hail fall in Azzano Decimo. From the satellite evolution shown in the "Sandwich" images (Setvák et al., 2012; Figures 6a-d), the storm of interest is evident moving SW to NE (e.g. compare the storm position in Figures 6a-d) in northeastern Italy. Apparently, the hailstones were produced (Figure 6b) just before the storm started to exhibit a distinct "plume" and overshooting top (Figures 6c,d) and hence before it reached its maximum strength, as inferred from satellite data.

Figure 7 shows both a 30-min evolution of cells in the Alpine domain from MSG IR satellite and collocated lightning data (both cloud-to-ground and cloud-to-cloud flashes) and a 10-min evolution from maximum radar reflectivity and lightning data. The lightning activity is particularly frequent along an instability line connecting NE Italy with Vienna (Figure 7, left panel), but in the entire Po Valley there is only one active cell, that seems to be isolated

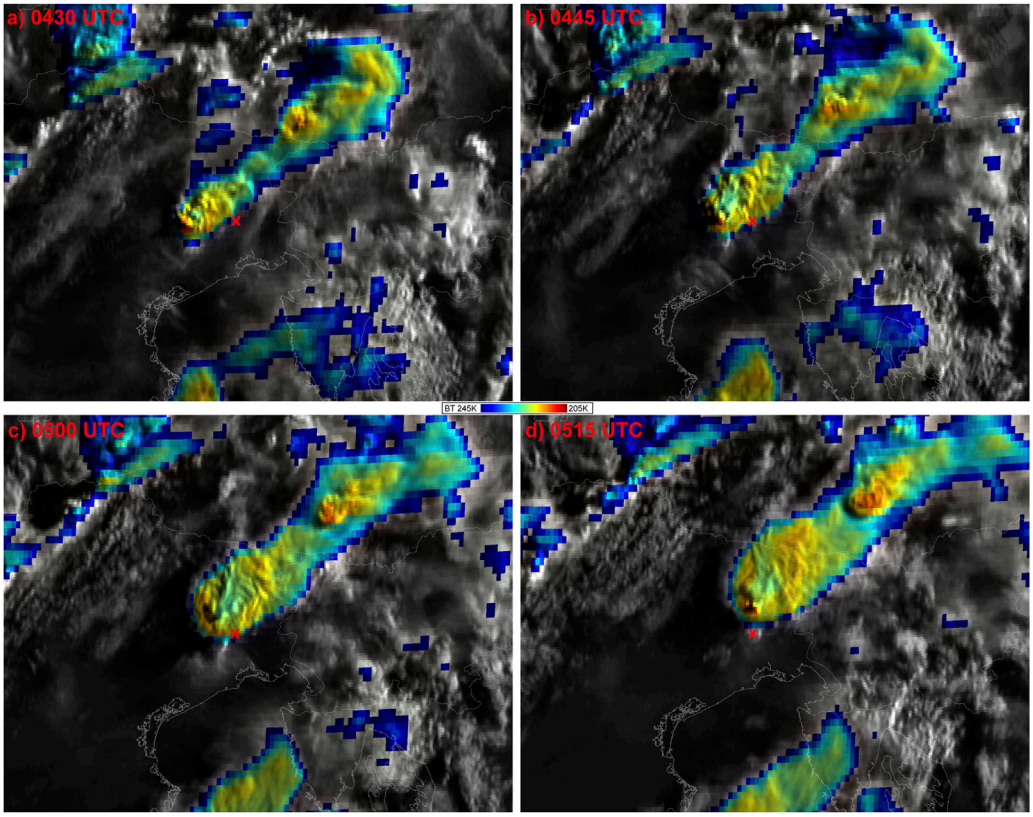

FIGURE 6
"Sandwich" images made from 10.3-μm infrared Brightness Temperature and visible channels of Eumetsat MSG satellite (see Setvák et al., 2012), showing northeastern Italy at **(a)** 0430, **(b)** 0445, **(c)** 0500, and **(d)** 0515 UTC. The red "x" shows the radiosounding location. Note that parallax effect has not been corrected, since this composite image mixes together clouds at different heights. Courtesy of Martin Setvák (CHMI).

and relatively small (Figure 7, right panel). The maximum 5-min rain accumulation (8.0 mm) recorded in nearby surface stations (Figure 7) was observed between 0440 and 0445 UTC, at Squarzere (9 km SW of Azzano Decimo), followed by 6.8 mm between 0435 and 0440 UTC in Porcia (12 km NW of Azzano Decimo), 5.2 mm between 0430 and 0435 UTC in Brugnera (15 km W of Azzano Decimo), and 4.1 mm between 0455 and 0500 in San Vito al Tagliamento (12 km E of Azzano Decimo). Since the cell movement was mainly from west to east, these heavy rainfall rates and timings confirm that the cell passed above Azzano Decimo at about 0450 UTC. The heavy rainfall and lightning recorded with the storm also exemplifies the multiple hazards produced by supercell storms (e.g., Markowski and Richardson, 2010).

3.3.2 Radar analysis

In this section we will analyze the observations made by the Fossalon di Grado radar. Figure 8 shows the evolution of the column-maximum reflectivity during the 20 min when the storm was approaching Azzano Decimo. The vertical projections (outset panels) show equivalent radar reflectivity factor Z values as high as 60 dBz associated with the cell above Azzano Decimo (labeled Azzano X) in the whole vertical column. Note that between 7 and 9 km AGL there appears to be some "gaps" in data in the vertical projections. That is due to the fact that the scanning strategy used by the radar at that time was using only 7 PPIs (plan position indicator) elevations, i.e., 1.0°, 2.0°, 3.0°, 4.5°, 8.0°, 14.9°, and 20.9°. In fact, since Azzano Decimo is about 65 km away from the radar, there is only a single elevation angle sampling between 6 and 12 km altitude, as visible in the reconstructed RHI (Figure 9a). Nonetheless, reflectivity values of 60 dBz up to nearly 10 km is consistent with the sample of giant-hail-producing storms reported in Blair et al. (2011), indicating a powerful storm capable of lofting plentiful and/or sizable hydrometeors to great altitudes.

Constant-altitude plan-position indicator (CAPPI) images of filtered (decluttered) Z, differential reflectivity Z_{DR}, and radial velocity V_r of the storm (Figures 10, 11) reveal classic indicators of supercells in the hail-bearing storm. These include a hook-echo-like appendage (Markowski, 2002, and references therein), and Z_{DR} arc (Kumjian and Ryzhkov, 2008) at low levels (implying strong low-level storm-relative winds), and midlevel cyclonic azimuthal shear associated with the supercell's defining mesocyclone. Interestingly, the low-level mesocyclone (inferred by azimuthal shear in the radial velocities) is rather weak. This is expected in environments without much vertical wind shear (e.g., Goldlacker and Parker, 2023), as suggested by the quasi-straight hodograph revealed in the proximity sounding launched at 05 UTC and the <5 m s^{-1} of 0 – 1-km shear in the 04 UTC ERA5 reanalysis-derived hodograph. There is also a three-body scattering signature (TBSS; Zrnić, 1987) evident particularly in Z_{DR} (which has not been filtered). The Z_{DR} field also shows differential attenuation, probably due to the presence of smaller melting hail (e.g.,

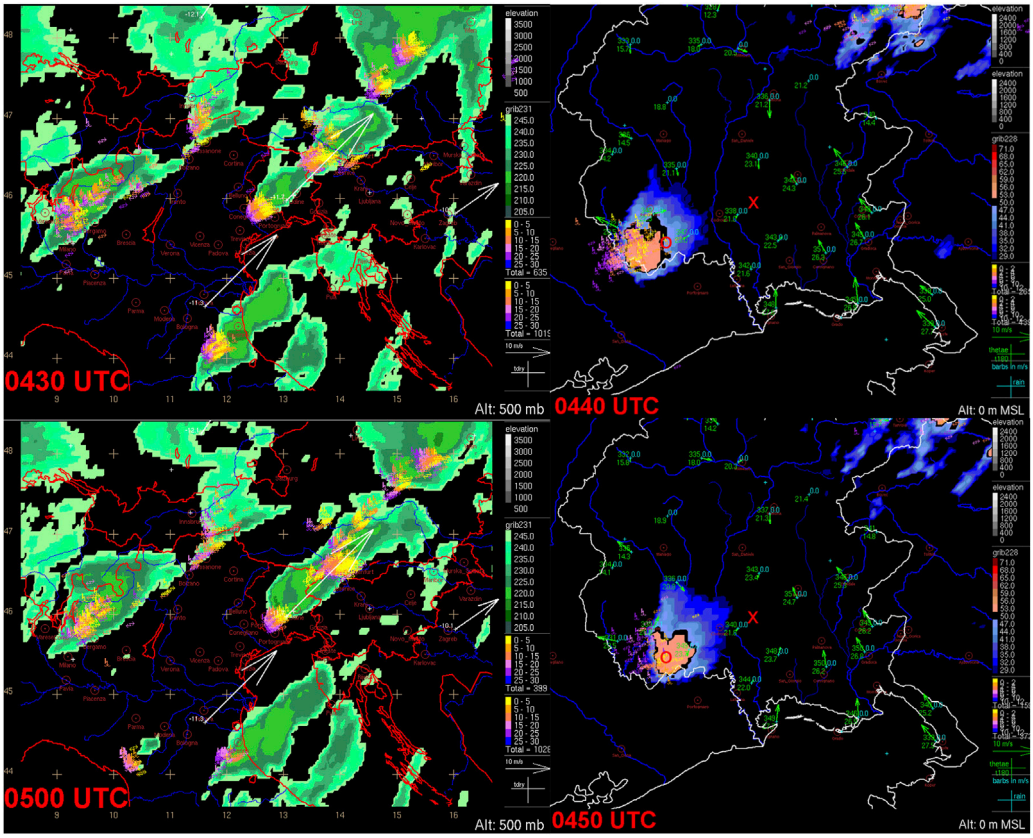

FIGURE 7
Left column: Eumetsat MSG InfraRed (10.8-μm) channel at 0430 (top) and 0500 (bottom) UTC, with cloud-to-ground and intra-cloud lightning observed by the Meteorage network (using Vaisala 7,002 sensors) in the time interval $\pm$ 15−min around the satellite time; white arrows indicate the wind observed by soundings at 500 hPa at about 2318 UTC of the previous day. Right column: Vertical maximum intensity of the Pasja Ravan radar (courtesy of ARSO) at 0440 and 0450 UTC with the same lightning data, but in the 12-min before the time of radar data and surface measurements (wind, Θ_e and 5-min rain accumulation), observed by a selection of FVG stations. Red "x" shows sounding base location, while red "o" shows the location where the 9 hailstones were collected.

Ryzhkov et al., 2013; Kumjian et al., 2019; Kumjian et al., 2024). Indeed, Figure 2b shows the presence of also small hailstones in the same garden where the large ones were collected.

Figure 12 shows Z and V_r taken directly from the Fossalon di Grado raw volume at 0450 UTC. When comparing the Z presentations at 1° elevation (about 1.2 km MSL) and 4.5° elevation (~5 km MSL), it is clear that the area encompassed by the Z echo increases with elevation, particularly on the southeast flank of the storm. This suggests the presence of an echo overhang or possible bounded weak echo region (BWER), indicating an updraft so strong that precipitation-sized hydrometeors cannot grow and/or are lofted. As mentioned above, the 1.0° elevation scan does not show signs of strong azimuthal shear, but rather mainly strong inflow winds. At 4.5° elevation, the V_r suggest the presence of both a mesocyclone and mesoanticyclone, which is unsurprising given the relatively straight hodograph at this time. Kumjian et al. (2021) found that anticyclonic vortex shedding from right-moving supercells led to increased updraft widths and larger hail formation in their simulations. That the radar data in this case display an anticyclonic shear region is at least consistent with these results, and to our knowledge has not been formally documented in association with a large hail event. (Unfortunately, the temporal resolution of radar data are insufficient to track these regions to ascertain whether or not this is an "anticyclonic vortex shedding" case as described in their paper.)

These radar depictions of the storm clearly suggest a powerful supercell capable of producing large hail. For comparison, Figure 13 shows PPIs from the record-breaking storm of 24 July 2023, also as it impacted Azzano Decimo. The PPIs show a more linear shape to the Z field at 1.0° elevation angle, and more circular above. However, the BWER seems to extend much deeper than in the 1 August 2021 storm, suggesting an even stronger updraft in the 24 July storm. The V_r PPIs show a mesocyclone at 1.0° and a stronger one at 4.5°, with folding showing inbound values in excess of 15 m s^{-1}. Overall, the radar features of the 24 July 2023 supercell are much more impressive than those visible in the raw radar data of 1 August 2021, suggesting an even more powerful storm was responsible for the record-breaking hailstone.

3.4 Hailstone internal structure analysis

In this section we present pictures of the nine hailstones that were thin-sectioned. Each of the hailstones was sectioned from one

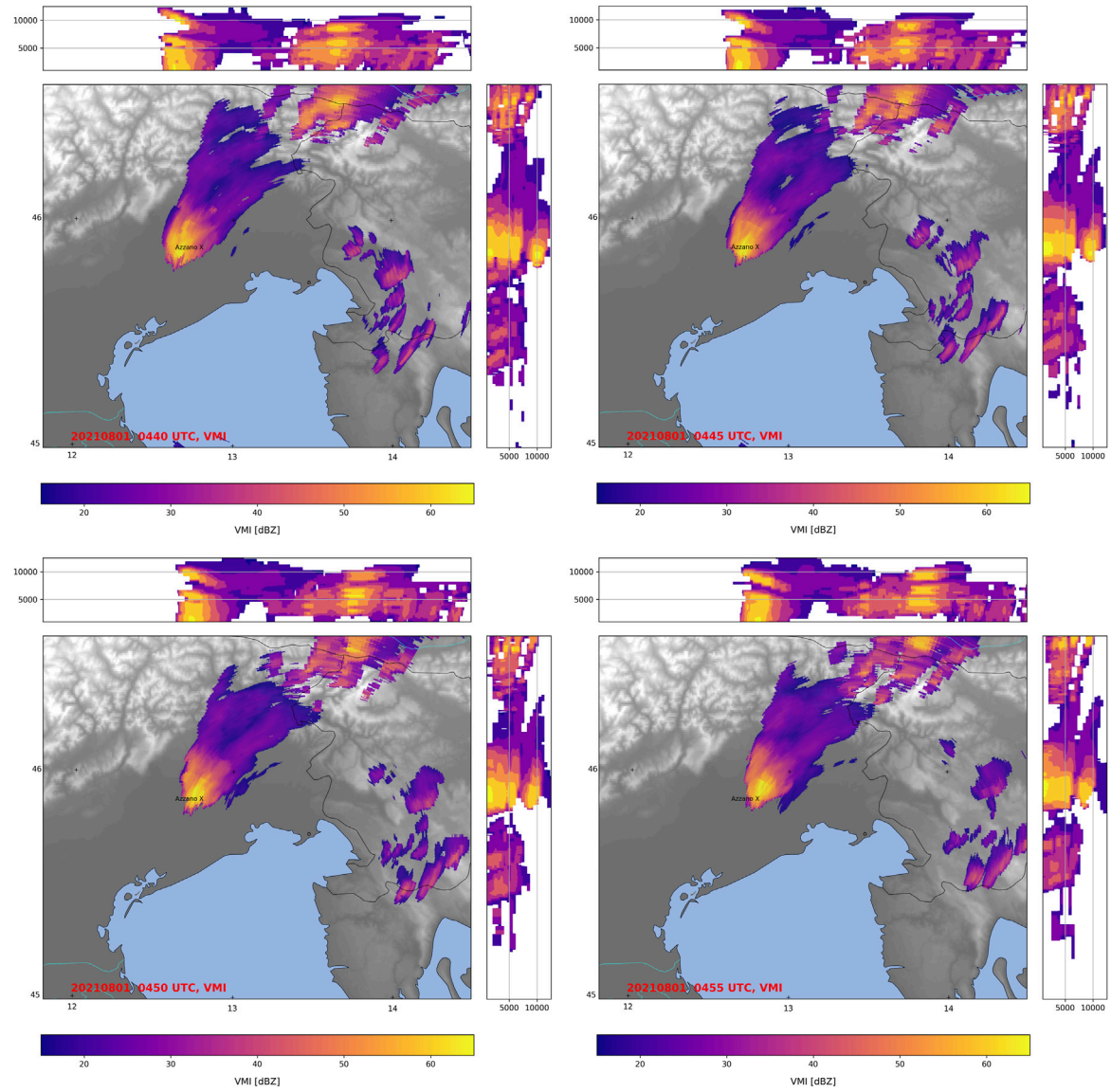

FIGURE 8
Vertical maximum reflectivity maps with lateral projections of maximum reflectivity from the Fossalon di Grado radar ("o" symbol) every 5 min from 0440 to 0455 UTC. The hailstones were collected in "Azzano X" village, which is marked in the map.

of the remaining halves of the originals, and thinned to between about 0.5 and 1 mm and photographed with transmitted light (photos on the left in Figure 14; Supplementary Figures S4–S7) and between crossed polarizing filters (photos on the right in Figure 14; Supplementary Figures S4–S7). All of the thin-section prints are at the same scale. In the transmitted light photographs, the dark areas are air pockets filled with ground ice from the sawing; light areas represent transparent ice, and grayish areas represent opaque ice. In S-5 (Supplementary Material Figure S5), the band saw blade came off its wheels while completing the thin-section cut, breaking the hailstone, so the photo is incomplete. A similar mishap happened during the sectioning of S-2 (Figure 14, top) and C-2 (Supplementary Figure S6, bottom) but otherwise the outer edges of the thin-sections are largely faithful to the shapes of the stones as collected. The large hailstones are highly nonspherical with prominent lobes, which is consistent with past studies of hailstone shapes (e.g., Knight and Knight, 1970b; Knight, 1986; Knight and Knight, 2005; Shedd et al., 2021). In particular, notice the exaggerated growth of single lobes along the long axis of hailstone C3 (Supplementary Figure S7, bottom row). Although such structures have been observed before, it is large enough to be puzzled by its origin. However, there is a hint of other lateral lobes beginning to form in hailstones S1 (Figure 14) and Supplementary Figure S3 (Supplementary Figure S4 bottom), suggesting that it is not a fluke. Notably, other giant and gargantuan hailstones have exhibited prominent elongated lateral lobes (e.g., the 18-cm Villa Carlos Paz stone reported in Kumjian and Co-authors, 2020).

All of the hailstones exhibit substantial wet growth outer layers, which seems to be a common characteristic of large hail (e.g., Knight and Knight, 2005; Kumjian and Co-authors, 2020). For example, Soderholm and Kumjian (2023) found that, across a sample of thin

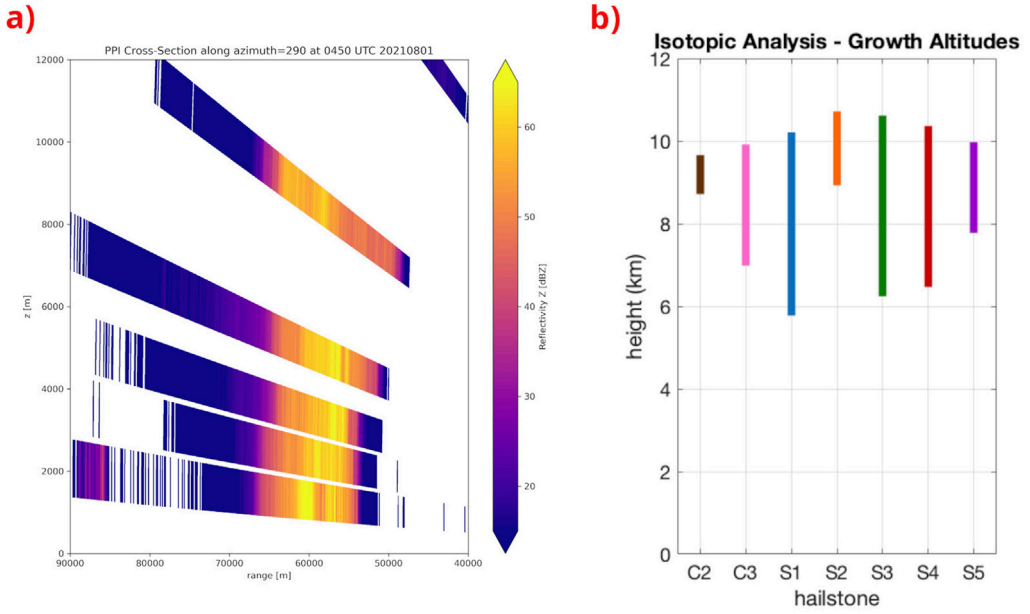

FIGURE 9
(a) Reconstructed RHI from all available reflectivity PPI scans (only 7 elevation angles collected as part of the operational scanning strategy) from the Fossalon di Grado radar on 1 August 2021 at 0450 UTC. Image constructed from data taken along the 290° azimuth, which intersects the hailstorm at about 60 km range. **(b)** The heights where each hailstone grew following the path estimated by the isotope analysis of Figure 17b.

sections of hailstones with varying sizes and shapes, 71% had a final wet growth layer that contributed >30% to the total wet growth area. This suggests that the final growth stage of large hailstones occurs at higher temperatures, consistent with the descending part of their trajectories (e.g., Kumjian and Lombardo, 2020).

Nearly all of the hailstones analyzed exhibit some growth layers with approximately symmetric ring structures suggestive of "symmetric tumbling," as opposed to random tumbling that would give rise to spherical symmetry (e.g., Knight and Knight, 1970a; Lin et al., 2024); C-4 (Supplementary Figure S7, top) is a particularly good example of such symmetric tumbling. The mirror-like symmetry of the internal structure along the major axis of the hailstone is suggestive of rapid spinning about its minor axis, which wobbles about the horizontal.

Also of note are the incomplete layering in hailstones S2 (Figure 14, top row, towards the hailstone's left side), S4 (Supplementary Figure S4, top row, towards the hailstone's top side), S5 (Supplementary Figure S5, in the middle-right and outer lower-left side), C2 (Supplementary Figure S6, bottom row, hailstone's right side), and C4 (Supplementary Figure S7, top row, left and right sides of hailstone). The latter could arise from the "symmetric tumbling" described above; However, other asymmetries suggest changes to the tumbling behavior that lead to preferential growth only on certain sides of the hailstones. In other words, hailstone falling behaviors can be highly complex (see the discussion in Lin et al., 2024).

The photographs of thin slices through crossed polarizing filters reveals the crystal fabric structure of hailstones (e.g., Knight and Knight, 1968). Often, there are large crystals found in the central parts of hailstones, as we have seen in other large hail from previous analyses (e.g., Knight and Knight, 2005). The thin sections show quite extensive recrystallization except in the bubbly layer–the small air bubbles in such layers inhibit grain boundary migration, which is the mechanism of grain coarsening. In particular, large single-crystal centers in C4 (Supplementary Figure S7); S1, S2 (Figure 14) are notable.

3.5 Hailstone water isotope analysis

Hailstone sampling involves cutting small pieces from each hailstone growth layer, melting each piece, and hermetically sealing it in a vial. The sampling was performed from the outside in. For each sample, a short note was written to describe where it was taken from the hailstone thick slice; these notes were later used to build the "composite" images shown in Figures 15, 16. A total of 28 samples were taken for the four "C" hailstones, and a total of 37 sampling were taken for the five "S" hailstones. Then, the 65 vials were then shipped to the Ice cores, Isotopic and Environmental Geochemistry Laboratory of the Ca' Foscari University of Venice to analyze their water isotopes with a Picarro cavity ringdown spectrometer[2].

Figures 15, 16 show the isotope ratios collocated with the approximate area along the hailstone cross section where the samples were extracted, scaled to cover the extent of the sampled fractions. Dotted lines refer to samples with possible evaporation issues (discussed below). There exists inter-hailstone variability in their radial isotopic profiles. For example, C2 (Figure 15, top right)

2 https://www.picarro.com/company/technology

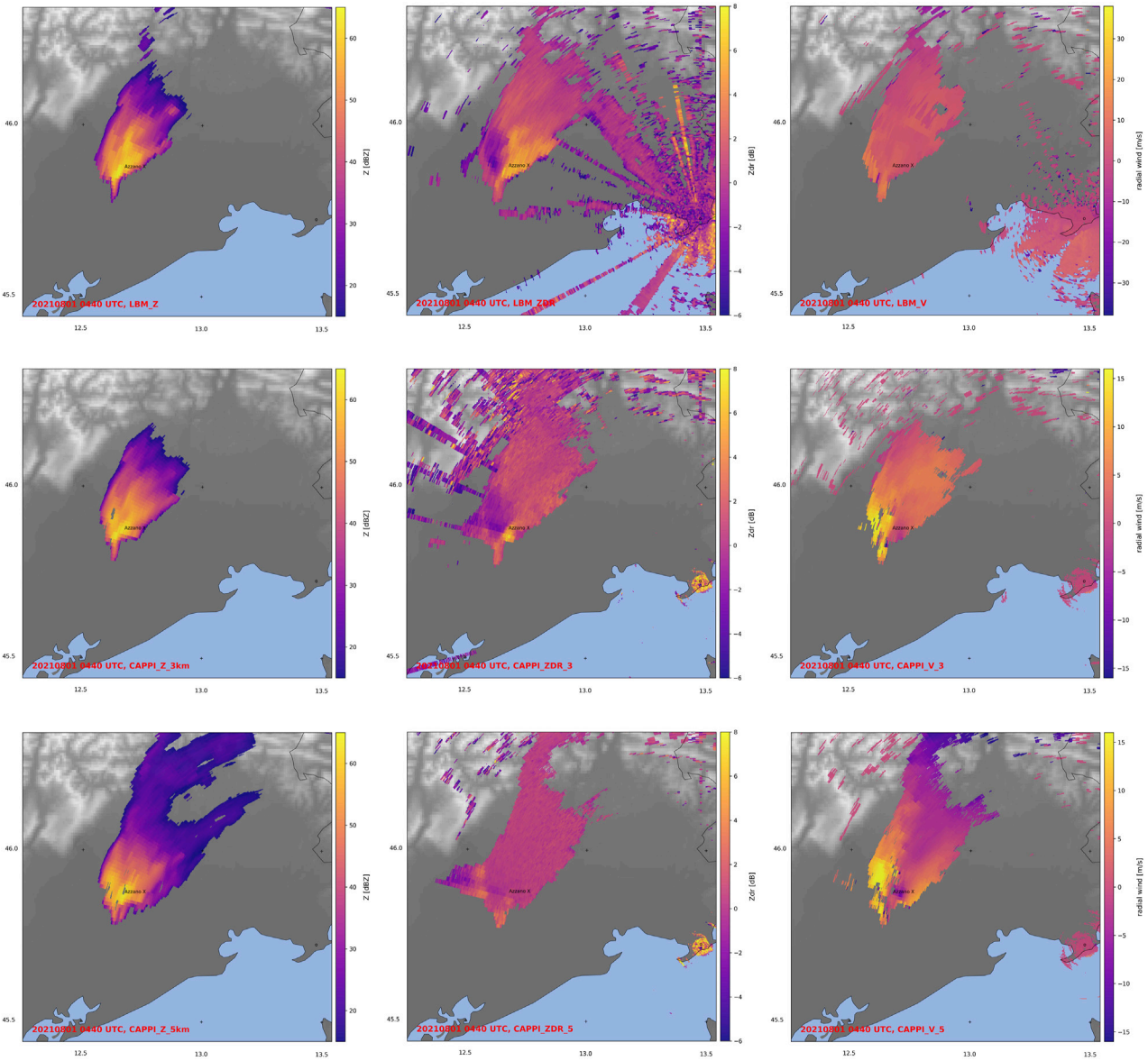

FIGURE 10
Z, Z_{DR} and radial wind V_r (respectively left, central, and right columns) at 0440 UTC of 1 August 2021 at the lowest beam PPI available (LBM, upper row) and at a constant altitude (CAPPI) of 3 km (central row) and 5 km (bottom row).

does not show much variability in δ^2H and $\delta^{18}O$ values in its different layers, whereas some (e.g., C3; Figure 15, bottom left) reveal considerable fluctuations. Where radial variation exists, generally, local minima (i.e., more negative δ^2H and $\delta^{18}O$ values) are found in the opaque ice, dry-growth layers, with greater values in the clearer, wet-growth ice. In addition, the hailstone centers generally exhibit less negative δ values than the adjacent fractions (e.g., Supplementary Figures S3,S4 in Figure 16, middle row). However, exceptions exist: Supplementary Figure S5 (Figure 16, bottom row) has somewhat greater δ^2H and $\delta^{18}O$ values in its outer wet-growth layer compared to its center.

The meteoric water lines describe the linear relationship between δ^{18}O and δ^2H in precipitation. On a global scale, this relationship is represented by the Global Meteoric Water Line (GMWL; Craig, 1961), which exhibits an approximate 8:1 slope between δ^{18}O and δ^2H, reflecting the relative proportions expected from equilibrium fractionation processes. The Local Meteoric Water Line (LMWL) derived for precipitation in Friuli Venezia Giulia for the period 1984–2015 (1,365 single sample, $R^2 = 0.98$) (Masiol et al., 2021) is given by Equation 1:

$$\delta^2H = 7.8\ [CI\ 7.7; 7.9] \cdot \delta^{18}O + 8.9\ [CI\ 8.3; 9.4] \quad (1)$$

with 95th percentile confidence intervals (CI) of Equation 1 calculated by ordinary nonparametric bootstrap resampling over 2000 replicates. The hail samples collected in this study plot almost exactly along the LMWL (Figure 17a), indicating that the formation of the hailstones occurred under near-equilibrium conditions. This interpretation is further supported by the deuterium excess or "d-

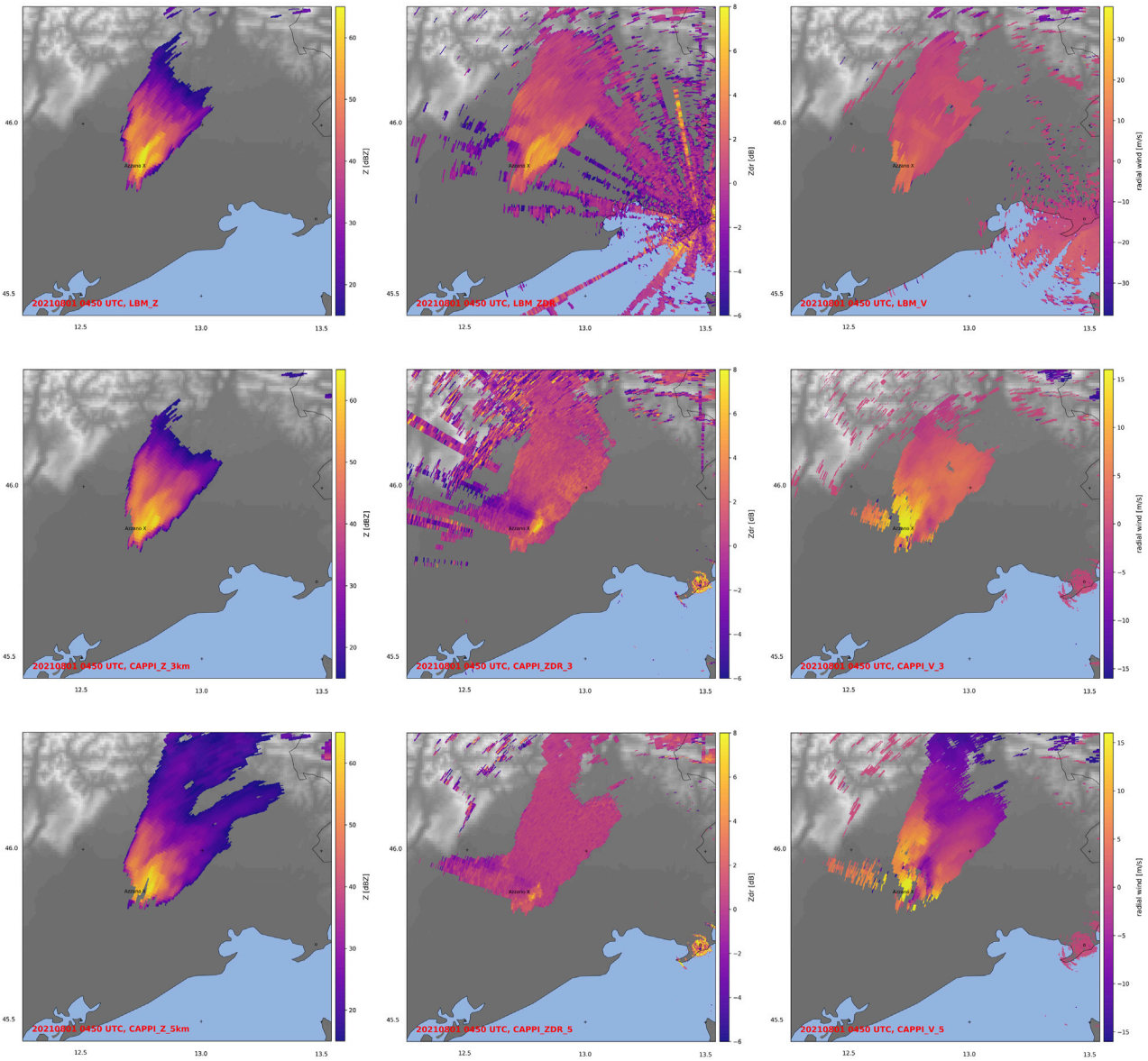

FIGURE 11
As the previous figure but at 0450 UTC of 1 August 2021.

excess" ($d = \delta^2H - 8\delta^{18}O$) values of the hailstone layers near the intercept value of the LMWL (Figures 15, 16). This also suggests the hailstones comprise water from a single source (almost certainly the Adriatic Sea, given the meteorological set up and the low-level inflow described in Section 3.1).

Nonetheless, several layers display markedly lower d-excess values, falling well below the LMWL line (Figure 17a) and suggesting partial evaporation effects during their formation. Some of those layers show very low d-excess values ($\ll$0‰) corresponding to remarkably high δ^2H and $\delta^{18}O$ values. The extremely low d-excess values are never located in the superficial layers but occur in the interior of the hailstones, lying between layers with normal values. This spatial pattern argues against post-sampling evaporation, metamorphism, or contamination, which would be expected to affect the outermost layers first and produce more systematic shifts in d-excess rather than isolated anomalies confined to the interior. Instead, these unusually low values most likely reflect specific conditions or processes acting during hailstone growth, rather than artifacts introduced after sampling.

Physically, d-excess is largely conserved during condensation but is highly sensitive to kinetic fractionation during evaporation, especially under dry, non-equilibrium conditions (Froehlich et al., 2002). In modern precipitation, very low or even negative d-excess values are typically associated with strong evaporation of raindrops or cloud droplets as they encounter warm, unsaturated air, where kinetic effects preferentially remove lighter isotopologues and drive the remaining vapor and condensate off the meteoric water line.

The combination of very low d-excess and relatively high δ^2H and $\delta^{18}O$ values may suggest episodes of intense kinetic

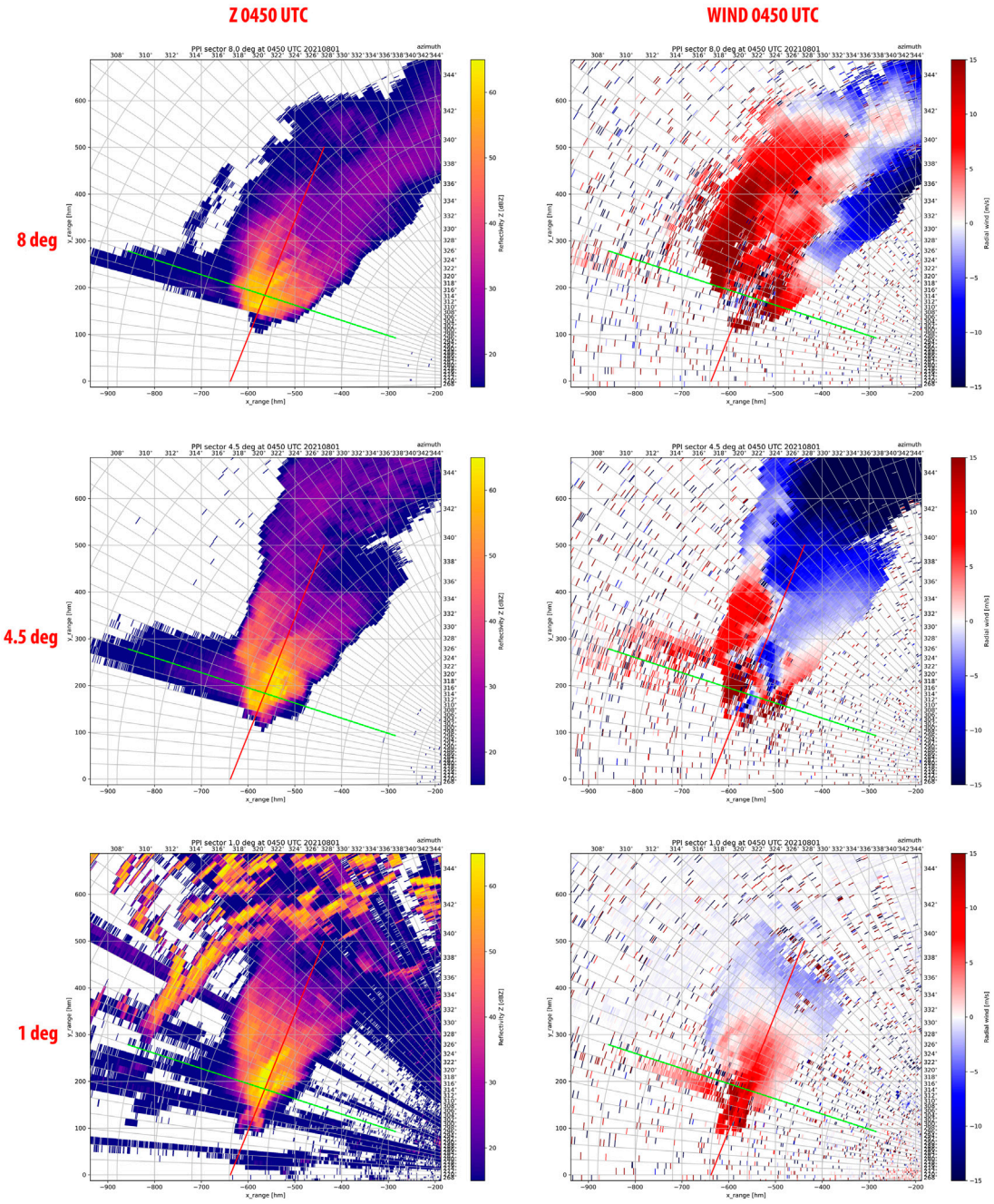

FIGURE 12
Three Fossalon di Grado radar PPI at 0450 UTC for the raw reflectivity Z (left column) and Doppler wind V_r (right column, with inward wind in blue and outward in red). Data from (bottom to top) 1.0°, 4.5°, and 8.0° elevation angles.

fractionation, perhaps occurring when liquid water on the growing hailstone surface underwent evaporation before being incorporated into the ice structure (see discussion in Section 2.2.2). Despite growing in cloudy conditions, hailstones undergoing wet growth have ~0 °C surface temperatures that can be much greater than the ambient environment, and thus the ambient vapor pressure is below what is needed to maintain that liquid in equilibrium, leading to evaporation. Further, this partially evaporated liquid water can also seep into porous rime ice and subsequently freeze, which may account for the opaque ice (dry growth) low d-excess layers. In addition, collection and subsequent freezing of raindrops (e.g., Kumjian and Lombardo, 2020) could lead to such low d-excess layers, particularly if the raindrops' journeys included sub-saturated conditions prior to being lofted into the hail growth region (Kumjian et al., 2014). However, even without considering those points far from the GMWL, there is a large variability of the isotopic values, with deuterium ranging from about −80‰ to −40‰ δ^2H of V-SMOW (Vienna Standard Mean Ocean Water, the global standard, i.e., the reference for isotopic analysis).

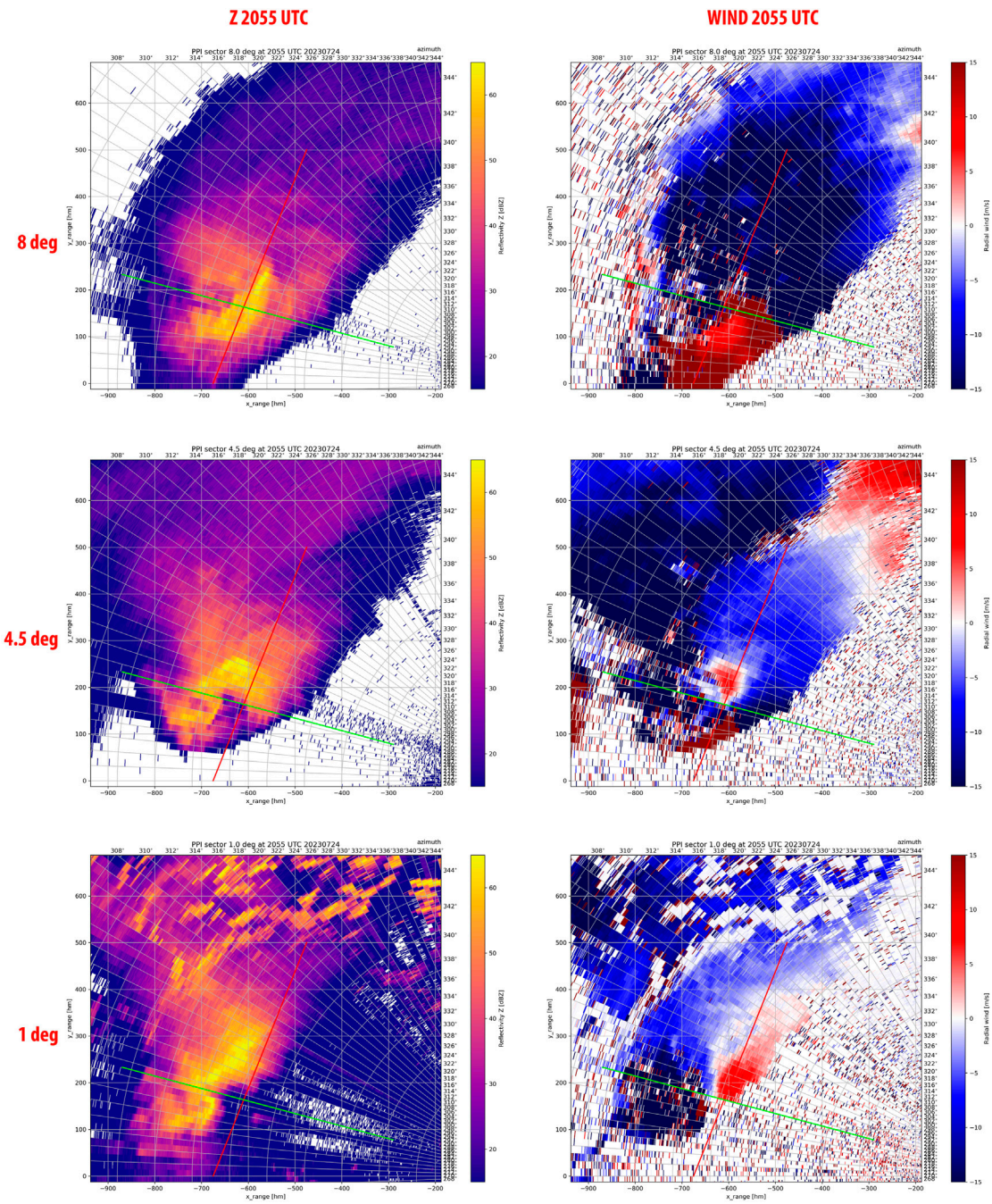

FIGURE 13
Three Fossalon di Grado radar PPI at 2055 UTC on 24 July 2023 for the (left column) reflectivity Z (in dBz) and (right column) Doppler velocity V_r in m s^{-1} (note the wind folding below −15 m s^{-1} at 4.5°). Elevation angles shown are (above) 1.0°, (middle) 4.5°, and (bottom) 8.0°.

Application of the "Jouzel" model (Jouzel et al., 1975; Jouzel et al., 1985), which relates a growth layer's isotope content to a specific atmospheric level (temperature), can provide at least qualitative insights into the hailstone's growth history in the mixed-phase region of the cloud. However, application of the model with the large isotope variability, including outlier points, causes the model to fail to converge. Given the kinetic fractionation issues (which invalidate the main assumptions of the Jouzel model outlined in Section 2.2.2), we removed the data from hailstones C1 and C4 (which had the most extreme outlier points) before applying the Jouzel model. Doing so allowed the model to converge, and the resulting profiles are shown in Figure 17b.

From this isotope analysis, one can infer that most of the hail growth seems to have occurred in the upper portions of the cloud, i.e., between 8 and 10 km, at temperatures between −16 and −31 °C. That result is consistent with the temperature profile and the estimate of homogeneous freezing level above 11 km made applying the Lifted Parcel Theory (cf. Figure 5), and with the

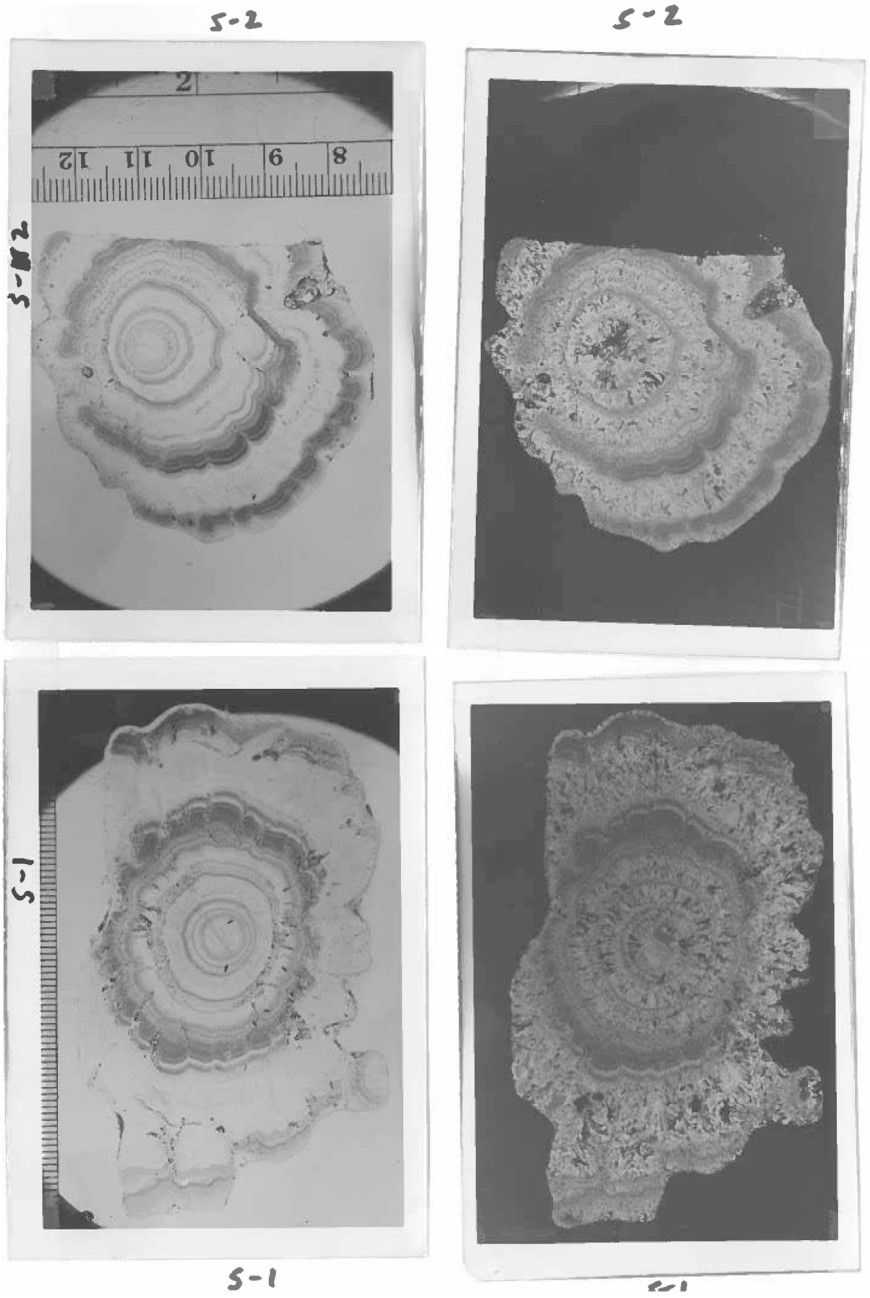

FIGURE 14
Thin slice of hailstones S-1 and S-2 (see Table 1). Photographs taken with normal light (left column) and cross-polarized light (right column). Similar pictures for the other hailstones are shown in Supplementary Figures S4–S7.

high radar reflectivity core (>55 dBZ) – a threshold indicative of hail–extending at least up to 10 km (Figure 9a), which corresponds well to the maximum growth height estimated from the isotopic analysis, as shown in Figure 9b. Thus, we infer that these particularly large hailstones have a relatively large residence time at high altitudes, which is consistent with the large vertical extent of high-reflectivity echoes discussed in Sections 3, 3.3. Further, the hailstones generally follow paths without multiple large vertical excursions, which is seemingly consistent with the simple, arching trajectories suggested by some modeling work (e.g., Dennis and Kumjian, 2017; Kumjian and Lombardo, 2020; Lin and Kumjian, 2022; Spychalla and Kumjian 2025b) and recent observations from Hailsondes (Soderholm et al., 2025). These results are also consistent with a similar analysis performed for hailstones collected in China (Lin et al., 2025).

Isotope analysis from the hailstone embryos (layer A in Figure 17b) show a wide range of formation temperatures from just below 0 °C to about −25 °C. Interestingly, the hailstones starting below 7 km reached a final size ≤7.5 cm, while those starting above 8 km reached a final size ≥7.0 cm. Hence, there is a moderate ($R = -0.6$) negative correlation between final hailstone size and embryo origination height, suggesting that the largest hailstones

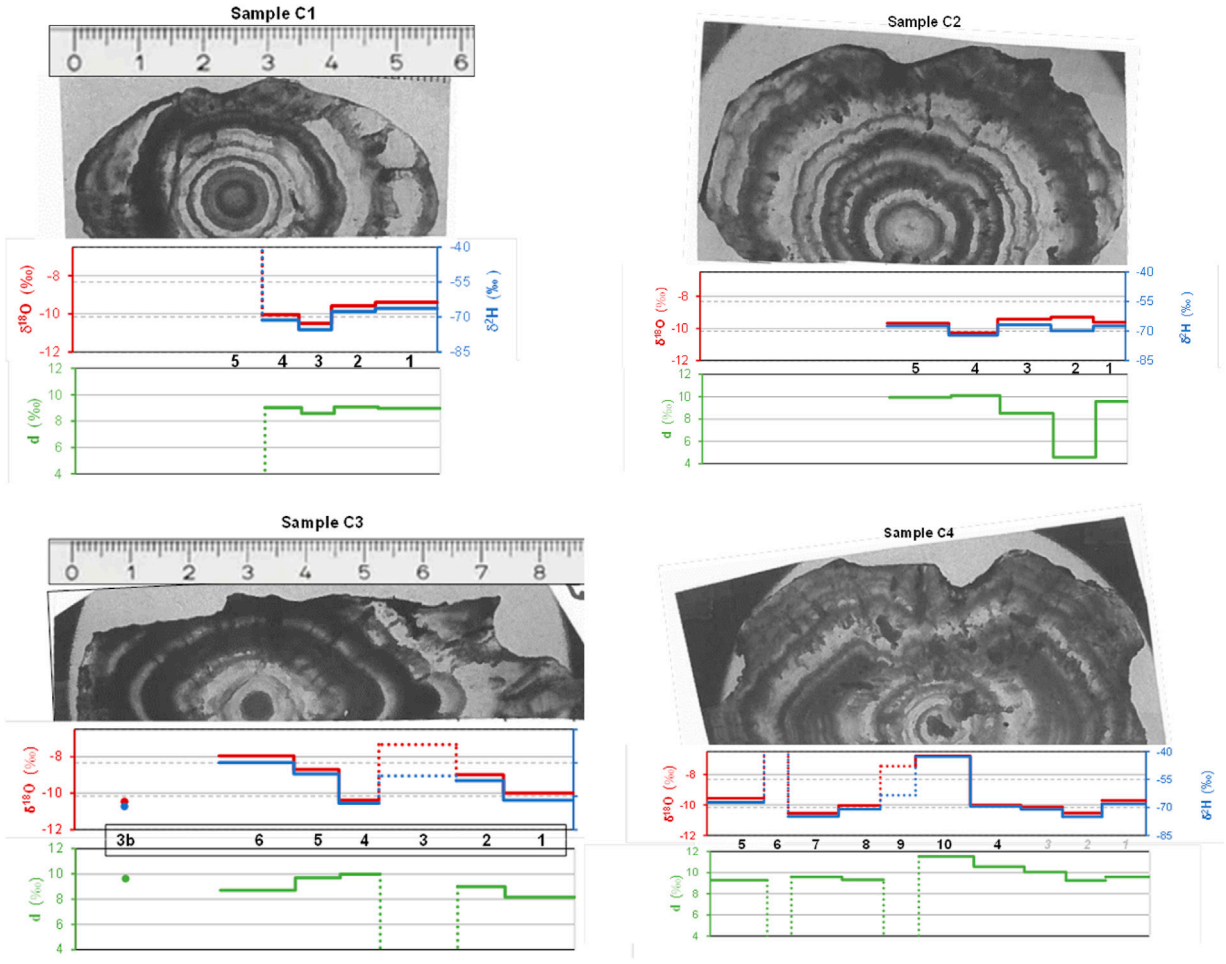

FIGURE 15
d, δ^{2H} and δ^{18O} values for each "C" hailstone specimens.

from this sample entered the updraft at lower altitudes and began their growth on ascent. Though the sample of hailstones is small and the size range is narrow, this finding seems consistent with results from a recent idealized modeling study by Spychalla and Kumjian. (2025a), who found that embryos initialized near the bottom of the hail growth zone had the greatest probability of producing the largest hail.

Lastly, an insoluble particle analysis were performed on two of these hailstones, but since they did not contain the embryos anymore (these were cut away during the isotope analysis) the results are shown only in the Supplementary Material (Section 1.2; Supplementary Figure S8).

4 Summary and conclusions

In the early morning of 1 August 2021, the village of Azzano Decimo was hit by a severe hailstorm, which produced considerable damage because of the large hail (up to ~10 cm in maximum dimension). The hailstorm was an isolated supercell that developed in an environment with very high potential instability: CAPE was of the order of 3,400 J kg^{-1} for the Rivolto sounding launched at 05 UTC. The extreme instability ranks amongst the top 10 ever recorded at that station, even if the exact value could be partially overestimated because the sounding was already contaminated by clouds above 750 hPa. The deep-layer shear was adequate for supercells, but the low-level shear was relatively weak, resulting from the low-level winds turning over time from east-northeast to south-southwest. The turned low-level winds made a straighter hodograph and aided in low-level moisture advection. In fact, between 0.1 and 0.6 km there is a strong vapor transport (Figure 4e), which brings the high-Θ_e air from the Adriatic Sea inland to feed the storm inflow (as the Θ_e-tongue discussed in Miglietta et al. (2016)). Additionally, strong mid-tropospheric winds combined with large vapor mixing ratio resulted in high vapor transport values, which De Martin et al. (2025) found to be supportive of storms producing large hailstones. We speculate that moister free troposphere help shield the storm's updraft from the negative effects of entrainment.

Remote-sensing observations of the storm revealed hallmarks of an intense, hail-producing supercell. This included multiple overshooting tops observed from satellite and a distinct above-anvil cirrus plume. Radar imagery revealed a bounded weak echo region (BWER) below 5 km altitude, a low-level hook echo, and a low-level Z_{DR} arc signature. Although the midlevel mesocyclone was present and robust, low-level

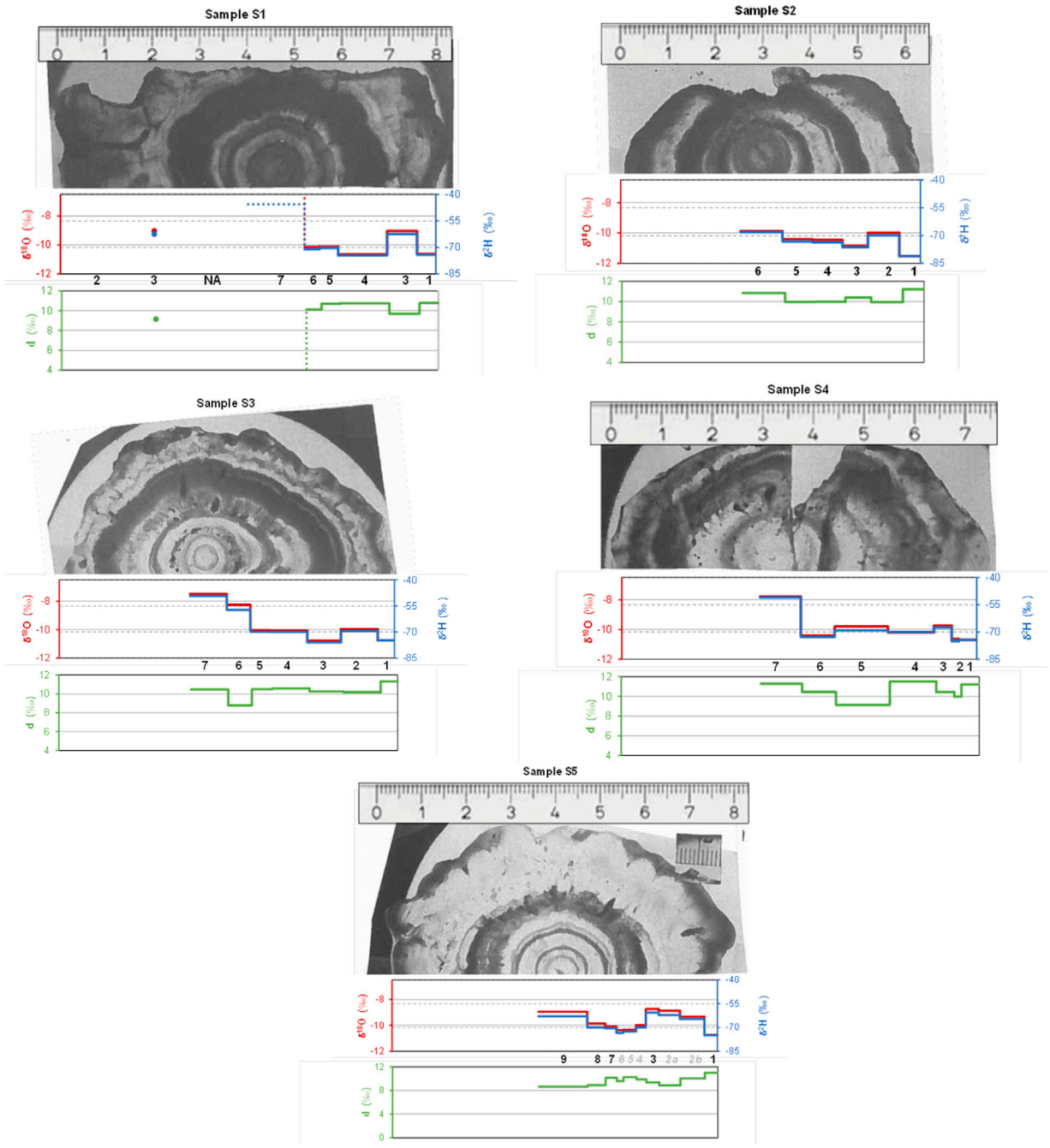

FIGURE 16
d, δ^{2H} and δ^{18O} values for each "S" hailstone specimens.

rotation was absent. The lack of a strong low-level mesocyclone can be explained by the weaker low-level shear in this case. In comparison, the hail European-record-breaking supercell of 24 July 2023 (which happened in the same village) exhibited a much deeper BWER and a stronger low-level (~1 km altitude) mesocyclone.

In Azzano Decimo, two observers (located ~2 km apart) collected samples of four and five hailstones, respectively, from their garden. The nine hailstones' internal structures were analyzed; the structures even within a single collection are characterized not by any evident uniformity, or commonality, in hailstone layering, but by a large variability. Sixty-five specimens taken from thick slices of these nine hailstones were analyzed with a high-precision Picarro spectrometer to characterize their water isotopic content. Results indicate that, although the water vapor likely came from a single source region (the Adriatic, based on the synoptic and mesoscale analyses), the isotopes within the hailstones also had large variability. This includes several internal layers with evidence of intense kinetic fractionation, likely owing to evaporation of liquid water either on the hailstone during wet growth or from raindrops that were subsequently collected. The Jouzel et al. (1975) model failed to associate each growing layer to a

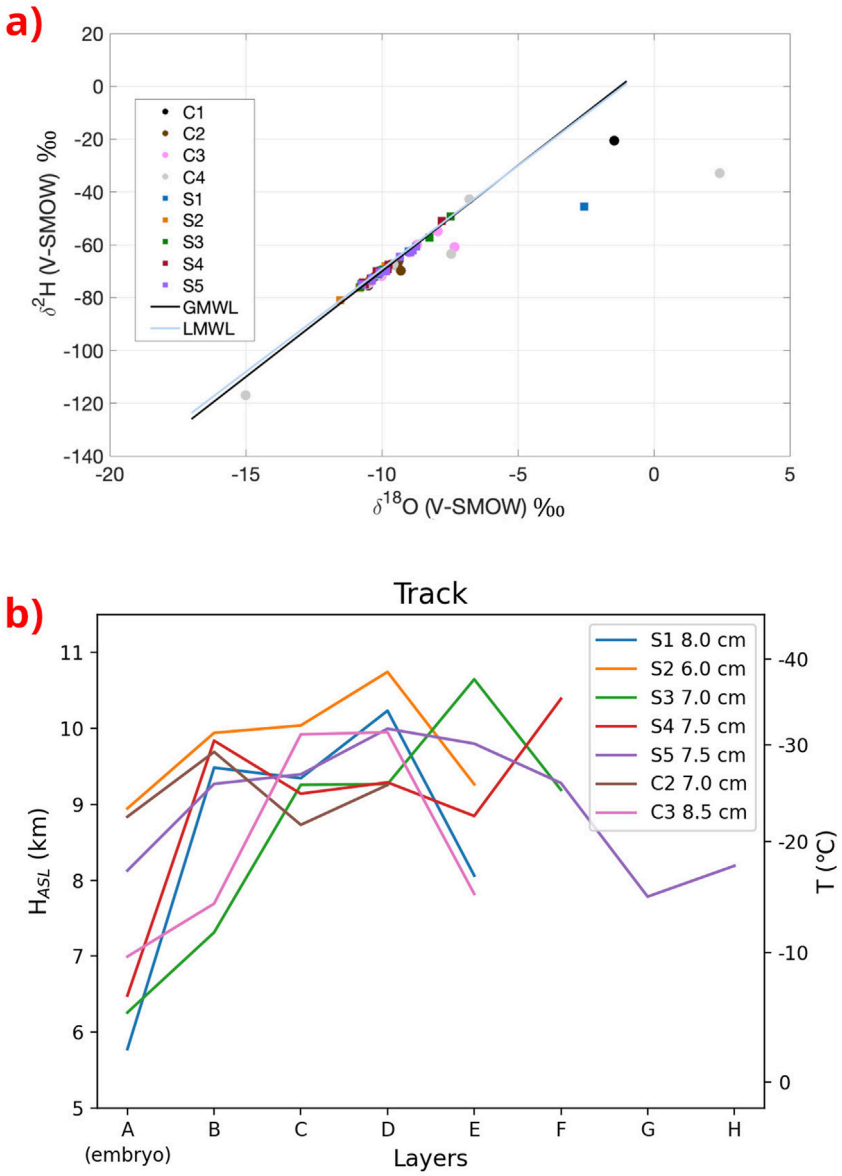

FIGURE 17
(a) δ^2H vs. $\delta^{18}O$ of the each hailstone specimens, labeled according to the legend. Overlaid are the Global Meteoric Water Line (GMWL, the reference) in black and the linear fit to the present data ("Local Meteoric Water Line" or LMWL, in blue). **(b)** Results of the Jouzel model applied to the hailstone isotope samples, with outliers C1 and C4 removed. Height (left scale) and temperature (right scale) of the growing layer is estimated based on the isotopic content within the samples.

specific altitude/temperature until removal of the isotope data from these two most extreme samples (C1 and C4). Considering only the other isotopes from the remaining seven stones, the Jouzel indicated that most of the hailstone growth happened at high altitudes (8–10 km), at temperatures between −16 and −31 °C. The relatively simple growth trajectories are consistent with previous modeling and observational work. An inverse correlation was found between the embryo origination altitude and final hailstone size, suggesting hail embryos introduced lower in the hail growth zone may grow to larger sizes. The relationship between temperature and altitude inferred from the Jouzel model also agree with the application of the simple 1-D "reversible adiabatic" lifting of the most unstable parcel applied at the Rivolto sounding with the "Tvc" method of Manzato and Morgan (2003). In fact, that method shows that the lifted parcel reaches temperatures below 0 °C above 5 km, below −10 °C above 7 km, and the homogeneous freezing level of −38 °C above 11 km. The altitude of this homogeneous freezing level is about 1-2 standard deviations above the mean from a large sample of significantly severe supercell environments, indicating a powerful storm.

Data availability statement

The data analyzed in this study is subject to the following licenses/restrictions: Requests to access these datasets should be directed to Inquiries for datasets of high-vertical resolution soundings should be

directed to Italian Aeronautica Militare (https://www.meteoam.it/it/disponibilita-dati). Radar data inquiries should be directed to FVG Civil Protection (https://monitor.protezionecivile.fvg.it/) for Fossalon di Grado radar and to ARSO (https://meteo.arso.gov.si/met/sl/weather/observ/radar/) for Pasja ravan radar. Hourly surface station data can be found online at https://www.osmer.fvg.it/archivio.php?ln=&p=dati, whereas 5-min data should be asked from https://www.osmer.fvg.it. Lightning data should be asked from Meteorage (https://www.meteorage.com/https://www.meteorage.com).

Author contributions

AM: Conceptualization, Formal analysis, Writing – original draft, Writing – review and editing, Data curation, Funding Acquisition. CK: Investigation, Formal Analysis, Writing – review and editing, Writing – original draft, Data curation, Methodology. MK: Conceptualization, Formal Analysis, Methodology, Visualization, Supervision, Writing – review and editing, Writing – original draft, Investigation, Resources. BS: Writing – original draft, Supervision, Writing – review and editing, Resources, Investigation, Formal Analysis. GD: Formal Analysis, Writing – review and editing, Investigation, Writing – original draft. MM: Writing – review and editing, Investigation, Formal Analysis, Visualization, Data curation, Software, Writing – original draft. QZ: Writing – original draft, Resources, Funding acquisition, Conceptualization, Supervision, Writing – review and editing, Methodology, Investigation. XL: Software, Writing – review and editing, Investigation, Writing – original draft, Formal Analysis, Data curation, Visualization. AH: Writing – review and editing, Writing – original draft, Funding acquisition, Conceptualization, Resources.

Funding

The author(s) declared that financial support was received for this work and/or its publication. This work was supported by the National Natural Science Foundation of China (Grant No. 42030607). MK was supported by grant AGS-2410918 from the U.S. National Science Foundation.

Acknowledgements

We thank Sara Santarossa and Michele Cristofoli, who collected and preserved the nine hailstones, and Rich Rotunno (NCAR, USA) for finding a way to send the hailstones from Italy to the United States. Francesco Sioni (OSMER - ARPA FVG, Italy) is acknowledged for Figure 3, Francesco De Martin (Univ. of Oklahoma, USA) is acknowledged for Figure 4e, and Martin Setvák (CHMI, Czech Republic) is acknowledged for Figure 6. Mirko Bertato (Civil Protection FVG, Italy) kindly provided the Fossalon di Grado radar data. Julian Alberto Giles and Kai Muhlbauer (Univ. Bonn, DE) helped with the Python wradlib library installation and developed the pseudo-RHI function. Joshua Soderholm (Australian Bureau of Meteorology), David Noone (University of Auckland Science Centre, New Zealand) and Adriana Raudzens Bailey (NCAR, USA) provided useful discussion on a very preliminary version of this work.

Conflict of interest

The author(s) declared that this work was conducted in the absence of any commercial or financial relationships that could be construed as a potential conflict of interest.

Generative AI statement

The author(s) declared that generative AI was not used in the creation of this manuscript.

Any alternative text (alt text) provided alongside figures in this article has been generated by Frontiers with the support of artificial intelligence and reasonable efforts have been made to ensure accuracy, including review by the authors wherever possible. If you identify any issues, please contact us.

Publisher's note

Supplementary material

The Supplementary Material for this article can be found online at: https://www.frontiersin.org/articles/10.3389/fenvs.2025.1735866/full#supplementary-material

References

Battaglioli, F., Groenemeijer, P., Púčik, T., Taszarek, M., Ulbrich, U., and Rust, H. (2023). Modeled multidecadal trends of lightning and (very) large hail in Europe and North America (1950–2021). *J. Appl. Meteor. Climatol.* 62, 1627–1653. doi:10.1175/JAMC-D-22-0195.1

Bechini, R., Gorgucci, E., Scarchilli, G., and Dietrich, S. (2002). The operational weather radar of fossalon di grado (gorizia, italy): accuracy of reflectivity and differential reflectivity measurements. *Meteor. Atmos. Phys.* 79, 275–284. doi:10.1007/s007030200008

Blair, S. F., Deroche, D., Boustead, J., Leighton, J., Barjenbruch, B., and Gargan, W. P. (2011). A radar-based assessment of the detectability of giant hail. *Electron. J. Sev. Storms Meteor.* 6 (7), 1–30. doi:10.55599/ejssm.v6i7.34

Craig, H. (1961). Isotopic variations in meteoric waters. *Science* 133, 1702–1703. doi:10.1126/science.133.3465.1702

De Martin, F., Manzato, A., Carlon, N., Setvák, M., and Miglietta, M. M. (2025). Dynamic and statistical analysis of giant hail environments in northeast Italy. *Q. J. R. Meteorological Soc.* 151, e4945. doi:10.1002/qj.4945

Dennis, E., and Kumjian, M. R. (2017). The impact of vertical wind shear on hail growth in simulated supercells. *J. Atmos. Sci.* 74, 641–663. doi:10.1175/jas-d-16-0066.1

Ehhalt, D. H., and Östlund, H. G. (1970). Deuterium in Hurricane Faith 1966: preliminary results. *J. Geophys. Res.* 75, 2323–2327. doi:10.1029/JC075i012p02323

Erdmann, F., Defer, E., Caumont, O., Blakeslee, R. J., Pédeboy, S., and Coquillat, S. (2020). Concurrent satellite and ground-based lightning observations from the optical Lightning Imaging sensor (ISS-LIS), the low-frequency network Meteorage and the SAETTA lightning Mapping Array (LMA) in the northwestern mediterranean region. *Atmos. Meas. Tech.* 13, 853–875. doi:10.5194/amt-13-853-2020

Friedman, I., Machta, L., and Soller, R. (1962). Water-vapor exchange between a water droplet and its environment. *J. Geophys. Res.* 67, 2761–2766. doi:10.1029/JZ067i007p02761

Froehlich, K., Gibson, J., and Aggarwal, P. (2002). *Deuterium excess in precipitation and its climatological significance*, 54–66.

Giaiotti, D., Gianesini, E., and Stel, F. (2001). Heuristic considerations pertaining to hailstone size distributions in the plain of friuli venezia giulia. *Atmos. Res.* 57, 269–288. doi:10.1016/s0169-8095(01)00080-1

Goldlacker, N. A., and Parker, M. D. (2023). Assessing the comparative effects of storm-relative helicity components within right-moving supercell environments. *J. Atmos. Sci.* 80, 2805–2822. doi:10.1175/JAS-D-22-0253.1

Grieser, J., and Hill, M. (2019). How to express hail intensity–modeling the hailstone size distribution. *J. Appl. Meteor. Climatol.* 58, 2329–2345. doi:10.1175/JAMC-D-18-0334.1

Hersbach, H., Bell, B., Berrisford, P., Hirahara, S., Horányi, A., Muñoz-Sabater, J., et al. (2020). The era5 global reanalysis. *Q. J. R. Meteorological Soc.* 146, 1999–2049. doi:10.1002/qj.3803

Jouzel, J., and Merlivat, L. (1984). Deuterium and oxygen 18 in precipitation: modeling of the isotopic effects during snow formation. *J. Geophys. Res.* 89, 11749–11757. doi:10.1029/jd089id07p11749

Jouzel, J., Merlivat, L., and Roth, E. (1975). Isotopic study of hail. *J. Geophys. Res.* 80, 5015–5030. doi:10.1029/JC080i036p05015

Jouzel, J., Merlivat, L., and Federer, B. (1985). Isotopic study of hail: the $\delta\, d - \delta\, 18o$ relationship and the growth history of large hailstones. *Quart. J. Roy. Meteor. Soc.* 111, 495–516. doi:10.1002/qj.49711146812

Knight, N. C. (1986). Hailstone shape factor and its relation to radar interpretation of hail. *J. Appl. Meteor. Climatol.* 25, 1956–1958. doi:10.1175/1520-0450(1986)025<1956:hsfair>2.0.co;2

Knight, C. A., and Knight, N. C. (1968). The final freezing of spongy ice: hailstone collection techniques and interpretations of structures. *J. Appl. Meteor. Climatol.* 7, 875–881. doi:10.1175/1520-0450(1968)007<0875:tffosi>2.0.co;2

Knight, C. A., and Knight, N. C. (1970a). The falling behavior of hailstones. *J. Atmos. Sci.* 27, 672–681. doi:10.1175/1520-0469(1970)027<0672:tfboh>2.0.co;2

Knight, C. A., and Knight, N. C. (1970b). Lobe structures of hailstones. *J. Atmos. Sci.* 27, 667–671. doi:10.1175/1520-0469(1970)027<0667:lsoh>2.0.co;2

Knight, C. A., and Knight, N. C. (2005). Very large hailstones from aurora, nebraska. *Bull. Amer. Meteor. Soc.* 86, 1773–1781. doi:10.1175/bams-86-12-1773

Knight, C. A., Ehhalt, D. H., Roper, N., and Knight, N. C. (1975). Radial and tangential variation of deuterium in hailstones. *J. Atmos. Sci.* 32, 1990–2000. doi:10.1175/1520-0469(1975)032<1990:ratvod>2.0.co;2

Kumjian, M. R., and Co-authors, (2020). Gargantuan hail in Argentina. *Bull. Amer. Meteor. Soc.* 101, E1241–E1258. doi:10.1175/BAMS-D-19-0012.1

Kumjian, M. R., and Lombardo, K. L. (2020). A hail growth trajectory model for exploring the environmental controls on hail size: model physics and idealized tests. *J. Atmos. Sci.* 77, 2765–2791. doi:10.1175/jas-d-20-0016.1

Kumjian, M. R., and Ryzhkov, A. V. (2008). Polarimetric signatures in supercell thunderstorms. *J. Appl. Meteor. Climatol.* 47, 1940–1961. doi:10.1175/2007jamc1874.1

Kumjian, M. R., Khain, A. P., Benmohse, N., Ilotoviz, E., Ryzhkov, A. V., and Phillips, V. T. J. (2014). The anatomy and physics of zdr columns: investigating a polarimetric radar signature with a spectral bin microphysical model. *J. Appl. Meteor. Climatol.* 53, 1820–1843. doi:10.1175/JAMC-D-13-0354.1

Kumjian, M. R., Lebo, Z. J., and Ward, A. A. (2019). Storms producing large accumulations of small hail. *J. Appl. Meteor. Climatol.* 58, 341–364. doi:10.1175/jamc-d-18-0073.1

Kumjian, M. R., Lombardo, K. L., and Loeffler, S. D. (2021). The evolution of hail production in simulated supercell storms. *J. Atmos. Sci.* 78, 3417–3440. doi:10.1175/jas-d-21-0034.1

Kumjian, M. R., Schrom, R. S., Soderholm, J., and Giammanco, I. (2024). "Radar and hail: advances in scattering, detection, and sizing," in *Advances in weather Radar. Volume 2: precipitation science, scattering and processing algorithms*. Editors V. N. Bringi, K. V. Mishra, and M. Thurai (London, United Kingdom: SciTech Publishing), 143–207.

Lebo, Z. J., Morrison, H., and Seinfeld, J. (2012). Are simulated aerosol-induced effects on deep convective clouds strongly dependent on saturation adjustment? *Atmos. Chem. Phys.* 12, 9941–9964. doi:10.5194/acp-12-9941-2012

Lin, Y., and Kumjian, M. R. (2022). Influences of CAPE on hail production in simulated supercell storms. *J. Atmos. Sci.* 79, 179–204. doi:10.1175/jas-d-21-0054.1

Lin, Y., and Kumjian, M. R. (2026). "How does low-level hodograph shape influence hail production?,"*J. Atmos. Sci.* submitted.

Lin, Y., Kumjian, M. R., Soderholm, J. S., and Giammanco, I. M. (2024). Modeling nonspherical hailstones. *J. Atmos. Sci.* 81, 1849–1881. doi:10.1175/JAS-D-23-0231.1

Lin, X., Zhang, H., Li, X., Zhang, Q., Heymsfield, A., Bi, K., et al. (2025). Isotopic analysis for tracing vertical growth trajectories of hailstones. *Adv. Atmos. Sci.* 42, 1195–1211. doi:10.1007/s00376-024-4211-x

Lombardo, K., and Kumjian, M. R. (2025). "The sensitivity of hail production in supercell storms to the distribution of vertical wind shear," in *12th European conference on severe storms* (Utrecht, Netherlands), ECSS2025–ECSS2187. doi:10.5194/ecss2025-187

Macklin, W. C., Merlivat, L., and Stevenson, C. M. (1970). The analysis of a hailstone. *Quart. J. Roy. Meteor. Soc.* 96, 472–486. doi:10.1002/qj.49709640909

Macklin, W. C., Knight, C. A., Moore, H. E., Knight, N. C., Pollock, W. H., Carras, J. N., et al. (1977). Isotopic, crystal and air bubble structures of hailstones. *J. Atmos. Sci.* 34, 961–967. doi:10.1175/1520-0469(1977)034<0961:icaabs>2.0.co;2

Manzato, A. (2012). Hail in ne Italy: climatology and bivariate analysis with the sounding–derived indices. *J. Appl. Meteor. Climatol.* 51, 449–467. doi:10.1175/jamc-d-10-05012.1

Manzato, A., and Morgan, G. (2003). Evaluating the sounding instability with the lifted parcel theory. *Atmos. Res.* 67-68, 455–473. doi:10.1016/s0169-8095(03)00059-0

Manzato, A., Cicogna, A., Centore, M., Battistutta, P., and Trevisan, M. (2022a). Hailstone characteristics in northeast Italy from 29 years of hailpad data. *J. Appl. Meteor. Climatol.* 61, 1779–1795. doi:10.1175/jamc-d-21-0251.1

Manzato, A., Serafin, S., Miglietta, M. M., Kirshbaum, D., and Schulz, W. (2022b). A pan-alpine climatology of lightning and convective initiation. *Mon. Wea. Rev.* 150, 2213–2230. doi:10.1175/MWR-D-21-0149.1

Manzato, A., Fasano, G., Cicogna, A., Sioni, F., and Pucillo, A. (2025). Relationships between environmental parameters and storm observations in po valley: are they climate change invariant?. *J. Appl. Meteorology Climatol.* 64, 267–298. doi:10.1175/JAMC-D-24-0034.1

Markowski, P. M. (2002). Hook echoes and rear-flank downdrafts: a review. *Mon. Wea. Rev.* 130, 852–876. doi:10.1175/1520-0493(2002)130<0852:hearfd>2.0.co;2

Markowski, P. M., and Richardson, Y. P. (2010). *Mesoscale meteorology in midlatitudes*. Wiley-Blackwell.

Masiol, M., Zannoni, D., Stenni, B., Dreossi, G., Zini, L., Calligaris, C., et al. (2021). Spatial distribution and interannual trends of $\delta^{18}O$, $\delta^{2}H$, and deuterium excess in precipitation across north-eastern Italy. *J. Hydrology* 598, 125749. doi:10.1016/j.jhydrol.2020.125749

Miglietta, M. M., Manzato, A., and Rotunno, R. (2016). Characteristics and predictability of a supercell during hymex sop1. *Quart. J. Roy. Meteor. Soc.* 142, 2839–2853. doi:10.1002/qj.2872

Morgan, G. M. (1973). A general description of the hail problem in the po valley of northern Italy. *J. Appl. Meteor.* 12, 338–353. doi:10.1175/1520-0450(1973)012<0338:agdoth>2.0.co;2

Morgan, G. M. (1992). Thetaplot, an equivalent potential temperature diagram. *Meteor. Atmos. Phys.* 47, 259–265. doi:10.1007/bf01025622

Nelson, S. P. (1983). The influence of storm flow structure on hail growth. *J. Atmos. Sci.* 40, 1965–1983. doi:10.1175/1520-0469(1983)040<1965:tiosfs>2.0.co;2

Nixon, C. J., Allen, J. T., and Taszarek, M. (2023). Hodographs and skew ts of hail-producing storms. *Wea. Forecast.* 38, 2217–2236. doi:10.1175/waf-d-23-0031.1

Nowotarski, C. J., Peters, J., and Mulholland, J. P. (2020). Evaluating the effective inflow layer of simulated supercell updrafts. *Mon. Wea. Rev.* 148, 3507–3532. doi:10.1175/MWR-D-20-0013.1

Punge, H. J., Bedka, K. M., Kunz, M., and Reinbold, A. (2017). Hail frequency estimation across Europe based on a combination of overshooting top detections and the era-interim reanalysis. *Atmos. Res.* 198, 34–43. doi:10.1016/j.atmosres

Ryzhkov, A. V., Kumjian, M. R., Ganson, S. M., and Khain, A. P. (2013). Polarimetric radar characteristics of melting hail. part i: theoretical simulations using spectral microphysical modeling. *J. Appl. Meteor. Climatol.* 52, 2849–2870. doi:10.1175/jamc-d-13-073.1

Setvák, M., Charvát, Z., Valachová, M., and Bedka, K. (2012). "Blended "sandwich" image products in nowcasting," in Proceedings of the 2012 EUMETSAT Meteorological Satellite Conference (Sopot, Poland).

Shedd, L. C., Kumjian, M. R., Giammanco, I. M., Brown-Giammanco, T., and Maiden, B. R. (2021). Hailstone shapes. *J. Atmos. Sci.* 78, 639–652. doi:10.1175/jas-d-20-0250.1

Smith, P. L., and Waldvogel, A. (1989). On determinations of maximum hailstone sizes from hailpad observations. *J. Appl. Meteor.* 28, 71–76. doi:10.1175/1520-0450(1989)028<0071:odomhs>2.0.co;2

Soderholm, J. S., and Kumjian, M. R. (2023). Automating the analysis of hailstone layers. *Atmos. Meas. Tech.* 16, 695–706. doi:10.5194/amt-16-695-2023

Soderholm, J. S., Kumjian, M. R., Brook, J. P., Peterson, A., Protat, A., Brimelow, J., et al. (2025). Measuring hail-like trajectories and growth with the hailsonde. *Bull. Amer. Meteor. Soc.* 106, E2128–E2142. in press. doi:10.1175/bams-d-24-0021.1

Spychalla, L., and Kumjian, M. R. (2025a). Uncoupling the impact of environment and updraft quantities on hail growth using an idealized hail model. *J. Atmos. Sci.* 82, 2102–2120. doi:10.1175/JAS-D-24-0234.1

Spychalla, L. K., and Kumjian, M. R. (2025b). An analytic approximation of vertical velocity and liquid water content profiles in supercell updrafts and their use in a novel idealized hail model. *J. Atmos. Sci.* 82, 2077–2099. doi:10.1175/JAS-D-24-0233.1

Taszarek, M., Allen, J. T., Púčik, T., Hoogewind, K. A., and Brooks, H. E. (2020). Severe convective storms across Europe and the United States. part ii: Era5 environments associated with lightning, large hail, severe wind, and tornadoes. *J. Clim.* 33, 10263–10286. doi:10.1175/JCLI-D-20-0346.1

van 't Veen, B., and Groenemeijer, P. (2025). "Optimizing c-band radar settings for mesocyclone and tornado detection," in *12th European conference on severe storms, Utrecht, the Netherlands, 17–21 Nov 2025. ECSS2025-287*. doi:10.5194/ecss2025-287

Warren, R. A., Richter, H., Ramsay, H. A., Siems, S. T., and Manton, M. J. (2017). Impact of variations in upper-level shear on simulated supercells. *Mon. Wea. Rev.* 145, 2659–2681. doi:10.1175/MWR-D-16-0412.1

Warren, R. A., Richter, H., and Thompson, R. L. (2021). Spectrum of near-storm environments for significant severe right-moving supercells in the contiguous United States. *Mon. Wea. Rev.* 149, 3299–3323. doi:10.1175/MWR-D-21-0006.1

Zrnić, D. S. (1987). Three-body scattering produces precipitation signature of special diagnostic value. *Rad. Sci.* 22, 76–86. doi:10.1029/RS022i001p00076